Fixed-time observer-based control of DFIG-based wind energy conversion systems for maximum power extraction

Pooyan Alinaghi Hosseinabadi[a, *], Hemanshu Pota[a], Saad Mekhilef[b], Howard Schwartz[c]

[a]School of Engineering and Information Technology, The University of New South Wales, Canberra, ACT, Australia
[b]School of Science, Computing and Engineering Technologies, Swinburne University of Technology, Hawthorn, VIC 3122, Australia
[c] Department of Systems and Computer Engineering, Carleton University, Ottawa, ON K1S 5B6, Canada,

Abstract

To extract maximum power from the available wind energy, it is necessary that the doubly-fed induction generator (DFIG) based wind energy conversion system (WECS) outputs that maximum power at each instant of time for different wind speeds. This can be achieved by controlling the rotor voltage of the DFIG. To make it possible, a novel maximum power point tracking (MPPT) controller in combination with state and disturbance observers and fixed-time stability notion is proposed in this paper. The sliding mode control (SMC) method is used to design the observer-based controller and ensure the robustness. The sliding mode state observer is designed while only the measurement of the stator reactive power and rotor speed is required. The modelling uncertainties and external disturbances are estimated by the sliding mode disturbance observer without information about their upper bounds in advance. Then, the combinatorial effect of uncertainties and disturbances are fully compensated by the designed controller. The fixed-time convergence issue is addressed where the bound on the settling time is user-defined using design parameters regardless of initial conditions. The elimination of chattering issue is considered in the design of the SMC laws. The stability analysis of the closed-loop system is obtained via the Lyapunov stability theory. The validity and robustness of the proposed method is tested in Simulink/MATLAB for a DFIG under two different scenarios of wind speed modelling. The proposed fixed-time method is also compared with a classical finite-time method. Comparing the results demonstrate that the proposed method outperforms the other method.
Keywords: DFIG, sliding mode, Fixed-time, WECS, observer, MPPT;

1. Introduction

1.1. Literature review and motivation

The power rating of commercially available WECS is increasing due to using DFIG as well as enhanced power electronic converters [1]. DFIG is one of the commonly utilized wind power generation systems in WECS because of its remarkable advantages, including high energy conversion efficiency from various wind speeds, the enhancement of the power quality, low converter cost, and minimum power losses compared with the systems with a fully fed synchronous generator with full-rated converters [2]. A comprehensive review has been made in [3] to compare the different DFIG models in the literature in terms of the impact of DFIG controls as well as short-circuit ratio on stability. An energy-shaping controller has been suggested in [4] for DFIG-based wind farm to mitigate sub-synchronous control interaction from the energy perspective. In [5], a robust feedback-linearized sliding mode controller has been designed for DFIG-based wind power plants to alleviate sub-synchronous control interaction. In [6], a fast frequency

response approach has been proposed for a DFIG based on variable power point tracking control to enhance the frequency stability.

One of the main control goals for DFIG based WECS is to optimally harvest the power of the wind turbine for different wind speeds, that is named MPPT [12]. Several approaches have been proposed for MPPT of DFIG based WECS, with each having its individual benefits and drawbacks. One of the most commonly used methods in the industry for MPPT of DFIG based WECS is a combined vector control (VC) with proportional-integral loops. Its key advantages are high reliability, decoupling reactive and active power control, and simple structure [7]. However, VC cannot give a consistent control performance once there are various operating conditions as the proportional-integral parameters are chosen by the one-point linearization, whereas DFIG based WECS is a nonlinear system. Due to the presence of uncertainties and nonlinearities in DFIG based WECS originating from random wind energy penetration as well as the wind turbine aerodynamics, a lot of nonlinear methods have been employed for MPPT of WECS. For example, in [8, 9], the backstepping control approaches have been designed for the nonlinear wind power systems. In [10], a nonlinear MPPT controller has been developed for DFIG based WECS where modal analysis has been used to reveal its better performance compared to VC.

Another effective nonlinear method found in the literature to deal with parametric uncertainties and nonlinearities as well as external disturbances is the SMC. It is well known that the SMC scheme can provide good robustness against perturbations with a strong disturbance rejection and fast response. In [11], the SMC approach has been considered to deal with the issue of the complexity of the DFIG based WECS and design a controller for reactive and active powers considering uncertainties. In [12], grid-connected rotor voltage has been calculated with no current control loops using SMC scheme for DFIG based WECS. However, the traditional sliding mode controller has a deficiency of chattering in the control signal due to the utilization of a discontinuous sign function, and this disadvantage often limits its applications [13]. In [14], the adaptive SMC method has been employed for DFIG based WECS to suppress the undesired impacts of uncertainties and reduce chattering issues. In [15], a chattering-free adaptive finite-time SMC has been proposed for WECS to control the generator speed in order to fulfill a MPPT. In [16], a comparison has been made in terms of chattering issues and robustness among high-order SMC method and PI control scheme first-order SMC for DFIG wind turbine. The results reveal that the high-order SMC approach outperforms the other two methods. In [17], the adaptive second-order SMC method has been proposed to reduce chattering for floating wind turbine considering collective blade pitch control. However, the complexity of parameters and structure of DFIG based WECS are more than the aforementioned floating wind turbines. In [18], a robust feedback-linearized SMC method has been proposed for DFIG-based wind farm where robustness to perturbation has been ensured by SMC and being independent of pre-specified operations has been ensured by feedback-linearization control. Although the experimental tests have been also verified the simulation results, there are no solution for reducing chattering issue and only asymptotic stability is proved in this paper.

The traditional SMC suffers an obvious problem, i.e., asymptotic convergence of the closed-loop system, owing to the employment of linear switching manifold [19, 20]. To cope with the disadvantages of asymptotic convergence, the terminal SMC (TSMC) approach has been suggested in [21] to realize finite-time convergence. In [22], the finite-time stability concept has been incorporated with second-order SMC scheme that outperforms the first-order SMC for tracking issue of the DFIG torque in terms of chattering reduction and robustness. In [23], a multivariable adaptive super-twisting SMC approach has been presented for DFIG based WECS to provide a finite time tracking of the optimal powers by smooth regulation of reactive and active powers quantities. However, the presented settling time using finite-time approaches relies on the system's initial conditions, which might limit its applications in practice due to likely unavailable initial conditions of the system. To handle this problem, the notion of fixed-time stability has been initially proposed in [24], which can guarantee that the settling time is bounded globally regardless of the system's initial conditions. The convergence time upper bound can be determined and adjusted by the design parameters irrespective of the system initial conditions. In [25], fixed-time stability notion has been integrated with a combined adaptive sliding mode controller-observer for the chaotic support structures for offshore wind turbines.

The upper bound of disturbances and uncertainties is required for SMC design that might be unavailable in practice. As a result, a lot of disturbance/perturbation observers-based controllers have been designed to cope with this issue. In [26], the observer-based adaptive disturbance rejection control has been designed to enhance the power tracking of DFIG based WECS with random wind speed. In [27], robust SMC utilizing nonlinear perturbation observer has been proposed for DFIG based WECS. The results demonstrate a better performance for the suggested scheme than VC,

SMC, and feedback linearization control. In [28], a new Kalman Filtering scheme has been designed as a disturbance observer for DFIG based WECS, where the estimated data has been used in the feedback controller. The high-gain state and perturbation observer (HGSPO) has been designed to approximate the uncertainties of multi-machine power systems [29]. However, an undesirable impact of the peaking phenomenon has been observed in HGSPO.

Furthermore, state observers can be alternatively used to produce an estimate of the system states and provide the estimated data in the control law. The system's output and input are used as the observer input [30]. The finite-time observers, including the Luenberger observer and Kalman filter, were introduced before late 1900 [31, 32] to apply for linear systems. The extended Kalman filter suggested for nonlinear systems was not able to deal with the issue of the system's parametric uncertainty [33]. Likewise, the nonlinear observers such as the backstepping approach [34], adaptive estimators [35], Hamiltonian scheme [36], as well as sub-Lyapunov exponents [37] could only guarantee the asymptotic convergence of the estimation errors [38]. Also, observer design for uncertain nonlinear systems has been challenging and slow because of the presence of the singular inputs in the nonlinear systems that makes them unobservable [39]. The finite-time sliding mode observers have been proposed to deal with the estimation issue of the unknown states and parametric uncertainties in a finite time and to provide robustness features [40]. A new fixed-time adaptive sliding mode observer based controller has been proposed in [25] to synchronize the support structures for offshore wind turbines considering disturbances and parametric uncertainties. In [41], an observer-based robust passivity-based controller has been designed for voltage source converter-based multi-terminal high-voltage direct current systems connected to an offshore wind farm. The uncertainties and external disturbances have been estimated using a linear perturbation observer and then, they have been compensated using a passive controller. A finite-time disturbance observer based SMC has been proposed in [42] for WECS with a permanent magnet synchronous generator to ensure MPPT in a finite time, alleviate chattering issue, and estimate and reject uncertainties and mechanical torque. In [43], sliding mode observer has been employed to provide the online estimation data of the DFIG's perturbation which is then compensated in real-time using a linear state feedback controller. In [27], the sliding-mode observer has been designed to estimate the perturbation of DFIG based WECS, and then the estimated data is compensated using SMC. However, the stability analysis for the closed-loop system using MPPT controller is not given in [27, 43].

Although the notion of finite-time stability has been successfully used to overcome finite-time convergence issues for MPPT of DFIG based WECS (such as [22, 23]), fixed-time stability notion is rarely applied for DFIG based WECS. As far as we know, only one research in the literature addressed the fixed-time convergence issue for MPPT of DFIG based WECS given in [44]. In this research, the upper bound of disturbances and uncertainties have been estimated using fixed-time adaptive estimator. However, this adaptive estimator (used in [44]) is only able to estimate the upper bound of uncertainties and disturbances, while the disturbance observer (given in our proposed method in [45]) can provide an accurate estimate of the uncertainties and disturbances resulting in decreasing their effects. Hence, the use of a disturbance observer (instead of an adaptive estimator) can effectively enhance the system stability [46] and tracking performance [47] by providing accurate estimated data in the control law of the SMC method. Also, by providing an accurate estimation of the uncertainties and disturbances in the control law, the controller is able to compensate their undesired effects more effectively. Subsequently, the switching gain in the control law would be reduced to a smaller value (compared with estimating the uncertainty upper bound) resulting in improving the robustness and reducing chattering [45, 48]. Additionally, in [44], a special form is considered for the upper bound of uncertainties and disturbances that might not be a comprehensive form. Another drawback of [44] is that their designed fixed-time state observer is discontinuous using the sign function. Thus, it might create chattering in the control signal in practice because the state observer law is utilized in the control law. To solve this issue, a sliding mode observer is suggested in this research where the integral of sign function appears in the state observer law [45]. Consequently, the observer and control signal will be smoother and chattering free.

Motivated with the aforementioned discussion and because of the complexity of this system and the presence of the strong nonlinearities originated from the wind turbine aerodynamics, together with the parameter uncertainties of the generator, and various wind speeds, a fixed-time robust nonlinear observer-based controller needs to be developed for MPPT of DFIG based WECS. This method requires overcoming the drawbacks of the relevant and existing methods (given in Table 1). Regarding the contribution of the proposed fixed-time observer-based controller in this research, a comparison is made in Table 1 among the proposed method in this research and the existing relevant methods in the literature for DFIG based WECS in terms of control key features.

Table 1. Comparison of theoretical.

Performance \ References	[7]	[8]	[11]	[12]	[14]	[16]	[22]	[17]	[23]	[27]	[44]	Proposed Scheme
Fixed-time convergence	×	×	×	×	×	×	×	×	×	×	✓	✓
Finite-time convergence	×	×	×	×	×	×	✓	✓	✓	×	✓	✓
Chattering alleviation	×	✓	×	✓	✓	✓	✓	✓	✓	×	×	✓
Obtaining stability analysis	×	×	✓	✓	✓	✓	✓	✓	✓	×	✓	✓
Robustness	×	✓	✓	✓	✓	✓	✓	✓	✓	✓	✓	✓
Considering disturbances	×	×	×	✓	✓	✓	✓	✓	✓	✓	✓	✓
Considering modelling uncertainties	×	✓	×	✓	✓	✓	✓	✓	✓	✓	✓	✓
No requirement of the upper bounds of disturbances and uncertainties	×	×	×	×	✓	×	×	×	✓	✓	✓	✓
System complexity	×	✓	✓	✓	✓	✓	✓	×	✓	✓	✓	✓
Combining state and disturbance observers-based controller	×	×	×	×	×	×	×	×	×	✓	×	✓

1.2. Objectives

The overall aim of this research is to maximize the energy extraction from the available wind energy with various speeds by DFIG based WECS. For this purpose, a maximum power point tracking realization needs to be fulfilled. Initially, the control problem is analyzed and then, optimal tip speed ratio (OTSR) control approach is used to obtain MPPT errors and formulate the problem mathematically. In order for us to achieve the overall aim of this research, there are the following specific objectives:

1. To develop a robust nonlinear sliding mode controller in combination with sliding mode state and disturbance observers and fixed-time stability notion where only the measurement of rotor speed and reactive power is required, and there is no information about the upper bounds of modelling uncertainties and external disturbances in advance.
2. To eliminate the destructive chattering phenomenon from the control signal (that is inherent issue with classical SMC because of using signum function in the SMC laws).
3. To obtain the fixed-time stability analysis of the closed-loop system using the observer-based controller via the Lyapunov stability theory considering the fact that the separation principle does not hold for nonlinear systems [49].
4. To evaluate the performance of the suggested fixed-time control scheme for a grid-connected DFIG based WECS in comparison with that of another classical finite-time control method in Simulink/MATLAB.

1.3. Contribution

As compared to the existing methods, the major contribution and novelty of this work can be summarized as follows:

- Designing a combined fixed-time observer-based controller method using the fixed-time stability notion, sliding mode control, and sliding mode state and disturbance observers.

- Estimating the system states using the proposed sliding mode state observer while only the measurement of reactive power and rotor speed is available.
- Estimating the external disturbances and modelling uncertainties using the proposed sliding mode disturbance observer without the knowledge of their upper bounds in advance and then, fully compensating their combinatorial effect by the designed sliding mode controller.
- Proposing a solution for eliminating chattering from the control signal by using integral of sign function in the design of SMC laws.
- Obtaining the fixed-time stability proof of the closed-loop system in both sliding phase and reaching phase by choosing a proper candidate Lyapunov function (considering the fact that the separation principle does not hold for nonlinear systems) as well as obtaining settling time function (which is independent of the system's initial conditions).
- Proving the robustness of the proposed method by considering modelling uncertainties and external disturbances in the stability analysis as well as testing the robustness in simulation by considering a specific model for external disturbances (which is added to the system at $t = 8(s)$ in both simulation scenarios) and modelling uncertainties.

1.4. Paper structure

This paper is organized as follows. In Section 2, the dynamic modelling of DFIG based WECS is given. Section 3 presents the research design. In this section, the main control problem of this research is initially analyzed and mathematically formulated. Then, the required mathematical preliminaries used for the controller design procedure are given. Finally, the proposed observer-based controller design is given, and the stability analysis for the closed-loop system utilizing the proposed approach and Lyapunov stability theory is obtained. In Section 4, the simulation results of the proposed method and the finite-time method are given and compared. In Section 5, the conclusions are provided.

2. Model of DFIG based WECS

The DFIG is a wound rotor induction generator. The stator is directly connected to a fixed frequency three-phase grid. The rotor winding is also connected to the grid via two bi-directional power converters (back-to-back ac/dc/ac voltage source converters). The output power is capable of being controlled via back-to-back converter control and pitch control. Due to the difference between the electrical and mechanical frequencies, the compensating current injected in the rotor current has a variable frequency [50]. As a result, the behavior and operation of the DFIG is governed using the converters and their controllers. The DFIG has two converters, the Grid Side Converter (GSC) and Rotor Side Converter (RSC), that can be independently controlled. The RSC duty is to control the output reactive and active power by controlling the rotor current control. The GSC duty is to maintain the voltage of the capacitance between two converters (i.e., controlling the DC link voltage) as well as the power factor of the DFIG utilizing the control of the reactive power exchanged with the grid. The principle of operation of the DFIG based WECS is illustrated in Fig. 1. In this figure, we have: ω_r is rotor speed; ω_s is synchronous speed; P_s is stator active power; P_r is rotor active power; P_g is grid power.
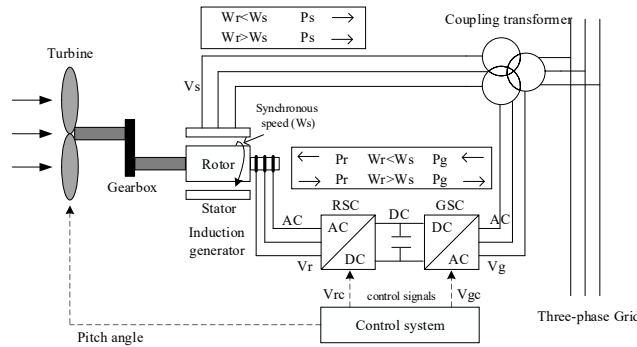
Fig. 1. A detailed configuration of the DFIG based WECS.

2.1. Wind turbine model

The mechanical power that the turbine can harvest is stated [51].

$$P_m = \left(\frac{1}{2}\right)\rho\pi R^2 v_{wind}^3 C_p(\lambda, \beta) \tag{1}$$

where ρ is density of the air; v_{wind} is the velocity of the wind; R is the rotor radius; $C_p(\lambda, \beta)$ is the power coefficient (or efficiency coefficient). Power coefficient C_p is a function of the blade pitch angle β and tip-speed-ratio (TSR) λ; where λ is defined as below

$$TSR = \lambda = speed \ of \ rotor \ tip/wind \ speed = \frac{\omega_m R}{v_{wind}} \tag{2}$$

where ω_m is the wind turbine rotational velocity. $C_p(\lambda, \beta)$ is expressed [52]

$$C_p(\lambda, \beta) = c_1\left(\frac{c_2}{\lambda_i} - c_3\beta - c_4\right)e^{-\frac{c_5}{\lambda_i}} + c_6\lambda \tag{3}$$

where we have,

$$\frac{1}{\lambda_i} = \frac{1}{\lambda + 0.08\beta} - \frac{0.035}{\beta^3 + 1} \tag{4}$$

where we have $c_1 = 0.5176$, $c_2 = 116$, $c_3 = 0.4$, $c_4 = 5$, $c_5 = 21$, and $c_6 = 0.0068$ [53]. In this research, the blade pitch angle β is considered as a constant for simplifying of the modelling of the wind turbine [54].

2.2. DFIG model

The generator dynamics have been given by [10, 52] as follows

$$\frac{di_{qs}}{dt} = \frac{\omega_b}{L_s'}\left(-R_1 i_{qs} + \omega_s L_s' i_{ds} + \frac{\omega_r}{\omega_s}e_{qs}' - \frac{1}{T_r\omega_s}e_{ds}' - v_{qs} + \frac{L_m}{L_{rr}}v_{qr}\right) \tag{5}$$

$$\frac{di_{ds}}{dt} = \frac{\omega_b}{L_s'}\left(-\omega_s L_s' i_{qs} - R_1 i_{ds} + \frac{1}{T_r\omega_s}e_{qs}' + \frac{\omega_r}{\omega_s}e_{ds}' - v_{ds} + \frac{L_m}{L_{rr}}v_{dr}\right) \tag{6}$$

$$\frac{de_{qs}'}{dt} = \omega_b\omega_s\left[R_2 i_{ds} - \frac{1}{T_r\omega_s}e_{qs}' + \left(1 - \frac{\omega_r}{\omega_s}\right)e_{ds}' - \frac{L_m}{L_{rr}}v_{dr}\right] \tag{7}$$

$$\frac{de_{ds}'}{dt} = \omega_b\omega_s\left[-R_2 i_{qs} - \left(1 - \frac{\omega_r}{\omega_s}\right)e_{qs}' - \frac{1}{T_r\omega_s}e_{ds}' + \frac{L_m}{L_{rr}}v_{qr}\right] \tag{8}$$

where ω_s is the synchronous angle velocity; ω_b is the electrical base velocity; ω_r is the rotor angle velocity; e_{ds}' and e_{qs}' are equivalent d-axis and q-axis (dq-) internal voltages; i_{ds} and i_{qs} are dq-stator currents; v_{ds} and v_{qs} are dq-stator terminal voltages; v_{dr} and v_{qr} are dq- rotor voltages; L_m is the mutual inductance; and the remaining parameters are given in [1, 10, 27, 52] as provided by Eqs. (13), (14), and (15). Note that the q-axis is aligned with stator voltage here, whereas the d-axis leads the q-axis. Thus, we have $v_{ds} \equiv 0$ and v_{qs} equals to the magnitude of the terminal voltage (i.e., $v_{qs} = v_s = 1$).

In addition, the stator reactive and active powers can be denoted by the stator currents and voltages as follows

$$P_s = v_{qs}i_{qs} + v_{ds}i_{ds} = v_{qs}i_{qs} \tag{9}$$

$$Q_s = v_{qs}i_{ds} - v_{ds}i_{qs} = v_{qs}i_{ds} \tag{10}$$

2.3. Shaft system model

The shaft system is modeled as a single lumped-mass system with the lumped inertia constant H_m, given in [55].

$$H_m = H_t + H_g \tag{11}$$

where H_g is the inertia constant of the generator and H_t is the inertia constant of the wind turbine. The electromechanical dynamics is provided as follows,

$$\frac{d\omega_m}{dt} = \frac{1}{2H_m}(T_m - T_e - D\omega_m) \tag{12}$$

where D is the lumped system damping; ω_m is the rotational speed of the lumped-mass system that is equal to the generator rotor speed ω_r; T_m signifies the mechanical torque that is as $T_m = \frac{P_m}{\omega_m}$. The numerical values of a grid-connected DIFG based WECS is given in [1, 10, 27, 52]. The system parameters are given as follows.

$$\omega_b = 100\pi \left(\frac{rad}{s}\right), \omega_s = 1.0 \ (p.u.), \omega_{r\_base} = 1.29, v_{s\_nom} = 1.0 \ (p.u.) \tag{13}$$

The DFIG parameters are given as follows.

$$P_{rated} = 5 \ (MW), \ R_s = 0.005 \ (p.u.), \ R_r = 1.1R_s, \ L_m = 4.0 \ (p.u.), \ L_{ss} = 1.01L_m, \ L_{rr} = 1.005L_{ss}, \ \acute{L}_s =$$
$$L_{ss} - \frac{L_m^2}{L_{rr}}, T_r = \frac{L_{rr}}{R_r}, R_1 = R_s + R_2, R_2 = \left(\frac{L_m}{L_{rr}}\right)^2 R_r \tag{14}$$

The wind turbine parameters are given as follows.

$$\rho = 1.225 \left(\frac{kg}{m^3}\right), R = 58.59(m^2), v_{wind.nom} = 12 \left(\frac{m}{s}\right), \lambda_{opt} = 6.325, H_m = 4.4(s), D = 0(p.u.) \tag{15}$$

3. Research design

Fig. 2 illustrates a schematic diagram of the proposed observer-based controller for MPPT applied to the RSC of DFIG based WECS. As this research concentrates on the MPPT objective, only the controller design for the RSC aims to be developed where the wind speed is considered to be below the rated value. The OTSR control approach is used, so the reference for rotor speed needs to be obtained for defining tracking errors for MPPT. The state and disturbance observers give the estimated data in the controller, and then the controller provides two control voltages to be applied to the RSC. This proposed sensorless controller requires the feedback of rotor speed and reactive power measurements. Also, there is no information about the upper bounds of external disturbances and modelling uncertainties in advance.
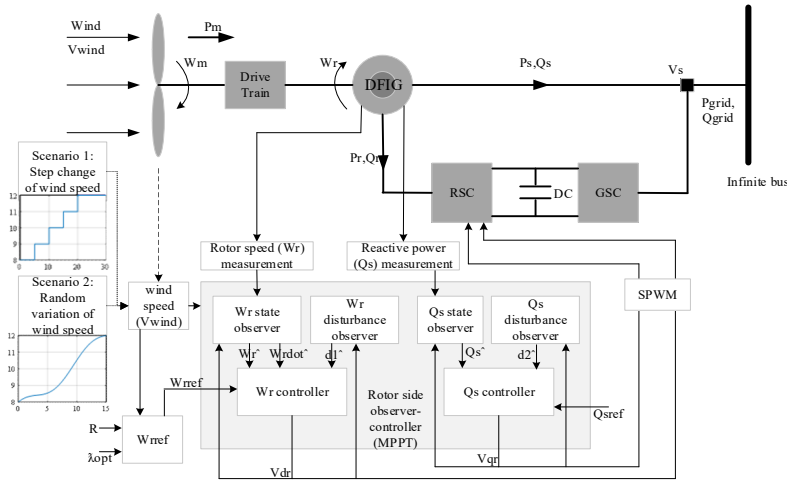

Fig. 2. Overall schematic of the proposed controller for RSC of DFIG.

3.1. Maximum power point tracking (MPPT)

The maximum power point is described as an operating point of the turbine at which maximum mechanical power would be harvested from the turbine [10]. It should be noted that this research aims to develop the MPPT observer-based controller for the RSC of DFIG based WECS, so the dynamics of the GSC are ignored. The maximum power extraction algorithms researched for WECS are classified into four main control approaches (elaborated in [44]), as follows. a) OTSR control; b) Optimal torque control; c) Hill-climb search control; d) Power signal feedback control. In this research, OTSR is used to obtain tracking error for MPPT and to formulate the problem. Note that the OTSR control approach regulates the generator's rotational speed to its reference in which TSR maintains at its optimal value to extract maximum power [56].

3.1.1 Problem formulation

Fig. 3 shows there are maximum values for $C_p(\lambda, \beta)$ with respect to TSR (λ) at different values of β. It can be observed that the maximum power coefficient $C_{p_{max}} \cong 0.48$ can be attained for the optimal TSR $\lambda_{opt} = 8.1$ and a fixed-pitch turbine $\beta \equiv 0$ for the grid-connected DFIG (given in Section 3 and [1, 10, 27, 52]).
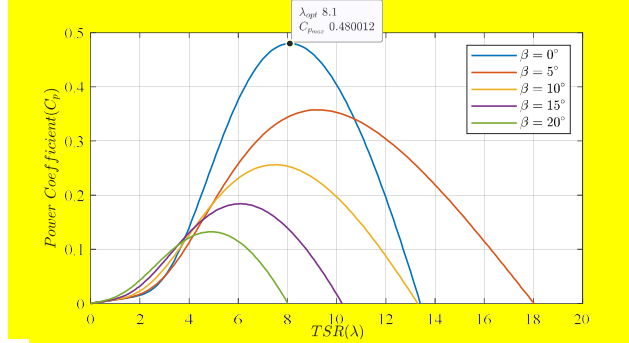

Fig. 3. Power coefficient (C_p) vs. TSR (λ) at different pitch angle values.

Fig. 4. displays mechanical power as a function of rotor velocity for a certain wind speed. The power for a certain wind velocity is maximum at the specific value of rotor velocity (called optimum rotor velocity). This is the speed which corresponds to optimum TSR (OTSR).
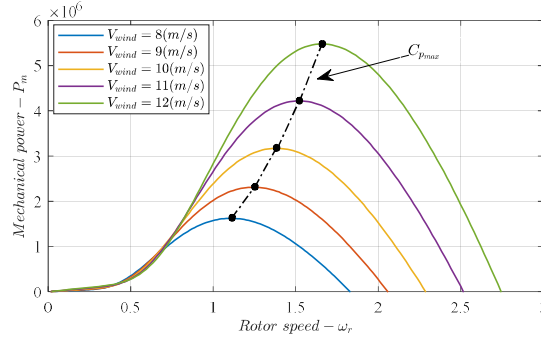

Fig. 4. Mechanical power (P_m) vs. rotor velocity (ω_r) at different wind speeds from $8(m/s)$ to $12(m/s)$.

Hence, the DFIG based WECS should be adjusted to operate at OTSR to ensure MPPT. Accordingly, the reference of rotor speed should be chosen such that TSR (λ) maintains its optimum value (which is the concept of OTSR control approach). That is, the MPPT can be achieved by adjusting λ given by (2) to its optimum value λ_{opt}. Obviously, the power coefficient C_p will be maximum $C_{p_{max}}$, when tip-speed-ratio λ is maintained to its optimum value λ_{opt} (see Fig. 3). Thus, the reference for the mechanical rotational speed will be as

$$\omega_{m_{opt}} = \frac{\lambda_{opt} v_{wind}}{R} \tag{16}$$

As a result, if ω_m reaches its optimum value $\omega_{m_{opt}}$, the maximum active power ($P_{s_{max}}$) will be obtained; i.e., if $\omega_m \to \omega_{m_{opt}} \Rightarrow P_s$ (the stator active power/the output electrical power) $\to P_{m_{max}}$. So, we have

$$P_{s_{max}} \approx P_{m_{max}} = \frac{1}{2\lambda_{opt}^3} \rho \pi R^5 C_{p_{max}}(\lambda_{opt}, \beta) \omega_{m_{opt}}^3 \tag{17}$$

As the rotational velocity of the lumped-mass system ω_m is equal to the generator rotor velocity ω_r, the MPPT can be achieved if the reference of the rotor speed $\omega_{r_{ref}}$ is chosen as $\omega_{r_{ref}} \approx \omega_{m_{opt}}$, while the stator reactive power Q_s is regulated to zero. Hence, we have

$$\begin{cases} \omega_{r_{ref}} \approx \omega_{m_{opt}} \\ Q_{s_{ref}} = 0 \end{cases} \tag{18}$$

So, MPPT realization can be achieved by considering the tracking error $e = [e_1 \ e_2]^T$ for stator reactive power Q_s and rotor speed ω_r as the outputs (using the concept of OTSR control). Thus, we have

$$\begin{cases} e_1 = \omega_r - \omega_{r_{ref}} \\ e_2 = Q_s - Q_{s_{ref}} \end{cases} \tag{19}$$

where we have $\omega_{r_{ref}} = \frac{\lambda_{opt}v_{wind}}{R}$ and $Q_{s_{ref}} = 0$ to achieve the unity power factor [10]. Differentiate the tracking error (19) until control input v_{dr} and v_{qr} clearly appeared, we obtain

$$\begin{bmatrix} \ddot{e}_1 \\ \dot{e}_2 \end{bmatrix} = \begin{bmatrix} f_1 - \ddot{\omega}_{r_{ref}} \\ f_2 - \dot{Q}_{s_{ref}} \end{bmatrix} + B \begin{bmatrix} v_{dr} \\ v_{qr} \end{bmatrix} \tag{20}$$

That can be rewritten as follows

$$\begin{cases} \dot{e}_1 = e_2 \\ \dot{e}_2 = f_1 + T_1 + d_1(t) + \Psi_1(x_1, x_2, x_3) - \ddot{\omega}_{r_{ref}} \\ \dot{e}_3 = f_2 + T_2 + d_2(t) + \Psi_2(x_1, x_2, x_3) - \dot{Q}_{s_{ref}} \end{cases} \tag{21}$$

where $d_1(t)$ and $d_2(t)$ are the model of matched external disturbances; $\Psi_1(x_1, x_2, x_3)$ and $\Psi_2(x_1, x_2, x_3)$ are modelling uncertainties. The sum of external disturbances and modelling uncertainties are considered as: $D_1 = d_1(t) + \Psi_1(x_1, x_2, x_3)$ and $D_2 = d_2(t) + \Psi_2(x_1, x_2, x_3)$. Also, we have

$$f_1 = \frac{\dot{T}_m}{2H_m} - \frac{1}{2H_m}\left\{w_b\left[\left(1 - \frac{\omega_r}{\omega_s}\right)\left(e'_{ds}i_{qs} - e'_{qs}i_{ds}\right) - \frac{1}{\omega_sT_r}\left(e'_{ds}i_{ds} + e'_{qs}i_{qs}\right)\right] + \frac{\omega_b}{\omega_s\acute{L}_s}\left[\frac{\omega_r}{\omega_s}\left(e'^2_{qs} + e'^2_{ds}\right) + \right.\right.$$
$$\left.\left. \omega_s\acute{L}_s\left(e'_{qs}i_{ds} - e'_{ds}i_{qs}\right) - R_1\left(e'_{ds}i_{ds} + e'_{qs}i_{qs}\right) - e'_{ds}v_{ds} - e'_{qs}v_{qs}\right]\right\} \tag{22}$$

$$f_2 = \frac{\omega_b}{\acute{L}_s}\left(R_1 i_{ds} + \omega_s\acute{L}_s i_{qs} - \frac{\omega_r}{\omega_s}e'_{ds} - \frac{1}{\omega_sT_r}e'_{qs}\right)v_{qs} + \frac{\omega_b}{\acute{L}_s}\left(\omega_s\acute{L}_s i_{ds} - R_1 i_{qs} - \frac{1}{\omega_sT_r}e'_{ds} + \frac{\omega_r}{\omega_s}e'_{qs} - v_{qs}\right)v_{ds} \tag{23}$$

Also, we consider $u_1 = v_{dr}$, $u_2 = v_{qr}$, and $B = \begin{bmatrix} b_1 & b_2 \\ b_3 & b_4 \end{bmatrix}$, then we obtain

$$T_1 = b_1 u_1 + b_2 u_2 \tag{24}$$

$$T_2 = b_3 u_1 + b_4 u_2 \tag{25}$$

$$u_1 = \frac{b_4 T_1 - b_2 T_2}{b_1 b_4 - b_3 b_2} \tag{26}$$

$$u_2 = \frac{b_3 T_1 - b_1 T_2}{b_2 b_3 - b_1 b_4} \tag{27}$$

Also, we have

$$b_1 = \frac{L_m\omega_b}{-2L_{rr}H_m}\left(\frac{e'_{ds}}{\acute{L}_s\omega_s} - i_{qs}\right) \tag{28}$$

$$b_2 = \frac{L_m\omega_b}{-2L_{rr}H_m}\left(\frac{e'_{qs}}{\acute{L}_s\omega_s} + i_{ds}\right) \tag{29}$$

$$b_3 = -\frac{L_m\omega_b}{\acute{L}_sL_{rr}}v_{qs} \tag{30}$$

$$b_4 = \frac{L_m\omega_b}{\acute{L}_sL_{rr}}v_{ds} \tag{31}$$

where B is the control gain matrix. As $\det(B) = -\frac{L_m^2\omega_b^2 v_{qs}}{2L_{rr}^2 H_m\acute{L}_s}\left(\frac{e'_{qs}}{\acute{L}_s\omega_s} + i_{ds}\right) \neq 0$ and it is invertible. The time derivative of T_m (given by (12)) is obtained as follows,

$$\dot{T}_m = \frac{\partial T_m}{\partial\omega_r} \times \frac{d\omega_r}{dt} + \frac{\partial T_m}{\partial v_{wind}} \times \frac{dv_{wind}}{dt} \tag{32}$$

where

$$\frac{\partial T_m}{\partial\omega_r} = \frac{1}{2}\rho A v_{wind}^3\left\{c_1 e^{-c5\left(\frac{v_{wind}}{\omega_r R}-0.035\right)}\left[\frac{c_5 c_2 v_{wind}^2}{R^2\omega_r^4} - \frac{(2c_2+0.035c_2c_5+c_4c_5)v_{wind}}{R\omega_r^3} + \frac{0.035c_2+c_4}{\omega_r^2}\right]\right\} \tag{33}$$

$$\frac{\partial T_m}{\partial v_{wind}} = \frac{1}{2}\rho A v_{wind}^2\left\{c_1 e^{-c5\left(\frac{v_{wind}}{\omega_r R}-0.035\right)}\left[-\frac{c_5 c_2 v_{wind}^2}{R^2\omega_r^3} + \frac{(4c_2+0.035c_2c_5+c_4c_5)v_{wind}}{R\omega_r^2} - \frac{0.105c_2+3c_4}{\omega_r}\right] - \frac{2c_6 R}{v_{wind}}\right\} \tag{34}$$

From now on, the control aim is to design the observer-based controller that guarantees converging the tracking errors given in (21) to zero within a fixed time and remains there afterward in the presence of unknown external disturbances and modelling uncertainties. Before proceeding with the design of the proposed method, some essential mathematical preliminaries that will be utilized for the design procedure are reviewed and provided in the following section.

3.1.2   *Mathematical preliminaries*

Some standard definitions and lemmas related to the fixed-time stability notion that will be utilized throughout this research are reviewed and given. The definition of global finite-time and fixed-time stability has been presented in [45, 57]. Given

$$\dot{x} = f(t, x) \tag{35}$$

where $x \in \mathbb{R}^n$ is the system state and $f : \mathbb{R}^n \rightarrow \mathbb{R}^n$ is a nonlinear function; t is time that is defined to be on the interval $[t_0, \infty)$, where $t_0 \in \mathbb{R}_+ \cup \{0\}$. The initial conditions of the system are $x(t_0) = x_0$.

Definition 1 ([58, 59]): The definition of the signum function is provided as below

$$sign(a) = \begin{cases} 1 & ; a > 0 \\ 0 & ; a = 0 \\ -1 & ; a < 0 \end{cases} \tag{36}$$

Moreover, the below relations are always true

$$\begin{cases} \frac{d|u|}{dt} = \dot{u} \times sign(u) \,; \dot{u} = \frac{du}{dt} \\ c \times sign(c) = |c| \\ |c \times sign(b)| \leq |c| \\ sign(a) \times sign(a) = 1 \end{cases} \tag{37}$$

where we have $a \in \mathbb{R} - \{0\}$ and $b, c \in \mathbb{R}$; $u \neq 0$ that is a differentiable function.

Definition 2 ([58]): The function of $sig(x)$ is defined as $sig^a(x) = |x|^a sign(x)$, where we have $a \in \mathbb{R}$. Note that $a \times sig^b(a) = |a|^{b+1}$ is always true.

Lemma 1 ([60]): For positive constants $a_1, a_2, \ldots, a_n \in \mathbb{R}$, and $0 < q < 2$ we obtain

$$(a_1^2 + a_2^2 + \cdots + a_n^2)^{\frac{q}{2}} \leq |a_1|^q + |a_2|^q + \cdots + |a_n|^q \tag{38}$$

Lemma 2 ([61]): Let $a_1, a_2, \ldots, a_n \geq 0$, $0 < b \leq 1$ and $c > 1$, we have

$$\sum_{i=1}^{n} a_i^b \geq (\sum_{i=1}^{n} a_i)^b, \sum_{i=1}^{n} a_i^c \geq n^{1-c}(\sum_{i=1}^{n} a_i)^c \tag{39}$$

Lemma 3 (Lyapunov characterization of fixed-time stability [62, 63]): Consider there exist four real numbers as $\rho_1, \rho_3 > 0$ and $0 < \rho_2 < 1 , \rho_4 > 1$, and a continuous radially unbounded $V(x): \mathbb{R}^n \rightarrow \mathbb{R}_{\geq 0}$ such that $V(0) = 0 , V(x) > 0 \,\forall\, x \neq 0$. If any solution $x(t)$ of (35) satisfies $\dot{V}(x) \leq -\rho_1 V^{\rho_2} - \rho_3 V^{\rho_4}$, then the origin of (35) is globally fixed-time stable and the settling time function is obtained as $T(x_0) \leq \frac{1}{\rho_1(1-\rho_2)} + \frac{1}{\rho_3(\rho_4-1)}$.

Lemma 4 ([64]): Consider a scalar system as below

$$\dot{y} = -\alpha y^{\frac{p}{q}} - \beta y^{\frac{m}{n}} , y(0) = 0 \tag{40}$$

where $\alpha, \beta > 0, q > p > 0, 0 < n < m < 2n$. Then, the equilibrium of (40) is fixed-time stable and the settling time T is bounded as follows

$$T \leq T_{max} := \frac{1}{\alpha}\frac{m}{m-n} + \frac{1}{\beta}\frac{q}{q-p} \tag{41}$$

3.2. Design of the fixed-time observer-based controller and stability analysis

A new fixed-time state and disturbance observers-based sliding mode controller (FOSMC) is designed for MPPT of DFIG based WECS. The FOSMC method is designed by incorporating sliding mode state and disturbance observers, sliding mode controller, and fixed-time stability notion where only the measurement of rotor reactive power and rotor speed is required. Before proceeding further with the design of the proposed scheme, it should be noted that the following assumptions are utilized in this research.

Assumption 1. The external disturbances and modelling uncertainties D_1 and D_2 (given in Eq. (21)) are bounded and unknown.

Assumption 2. ω_r fulfills $|\omega_r| \leq \eta_1$, and $\dot{\omega}_r$ fulfills $|\dot{\omega}_r| \leq \eta_2$, where η_1 and η_2 are known positive constants.

Assumption 3. The following inequalities holds.

$$\begin{cases} |f(t, \hat{x}) - f(t, x)| \leq \delta_1 \\ |\dot{f}(t, \hat{x}) - \dot{f}(t, x)| \leq \delta_2 \end{cases} \tag{42}$$

where δ_1 and δ_2 are known positive functions for all t. Note that we have $x = [x_1, x_2, x_3]^T = [\omega_r, \dot{\omega}_r, Q_s]^T$, $\hat{x} = [x_1, \hat{x}_2, x_3]^T = [\omega_r, \dot{\hat{\omega}}_r, Q_s]^T$, $u_1 = v_{dr}$, $u_2 = v_{qr}$, $f(t, x) = [f_1, f_2]^T$, and $f(t, \hat{x}) = [\hat{f}_1, \hat{f}_2]^T$.

Remark 1. It is worth mentioning that assumptions 1, 2, and 3 are common restrictive conditions for designing the observer-based controller for nonlinear systems that have been widely used in many practical publications such as [65-67].

The tracking error is considered as $e_i = x_i - x_{i_{ref}}$ (given by (19)), and its estimation is as $\hat{e}_i = \hat{x}_i - x_{i_{ref}}$. The error of state observer is defined as $\tilde{x}_i = \hat{x}_i - x_i$. The tracking errors of disturbance observers are defined as

$$Z_1 = h_1 - q_1 \tag{43}$$

where $q_1 = \dot{x}_1 - \int p_1 dt$ and $p_1 = \hat{f}_1 + T_1$, so we obtain $\dot{h}_1 = \hat{D}_1$. Also, we have

$$Z_2 = h_2 - q_2 \tag{44}$$

where $q_2 = x_3 - \int p_2 dt$ and $p_2 = \hat{f}_2 + T_2$, so we obtain $\dot{h}_2 = \hat{D}_2$. The sliding surfaces are considered as follows,

$$\begin{cases} s_1 = \dot{e}_1 + A_1(e_1) + B_1(e_1) \\ s_2 = \dot{s}_1 + A_2(s_1) + B_2(s_1) \\ s_3 = \dot{e}_3 + A_3(e_3) + B_3(e_3) \\ \sigma_1 = \dot{\tilde{x}}_1 + A_4(\tilde{x}_1) + B_4(\tilde{x}_1) \\ \sigma_2 = \dot{\tilde{x}}_3 + A_5(\tilde{x}_3) + B_5(\tilde{x}_3) \\ \xi_1 = Z_1 + \int A_6(Z_1)dt + \int B_6(Z_1)dt \\ \xi_2 = Z_2 + \int A_7(Z_2)dt + \int B_7(Z_2)dt \end{cases} \tag{45}$$

where we have $A_j(\varrho) = a_j \varrho^{\frac{p_j}{q_j}}$, $B_j(\varrho) = b_j \varrho^{\frac{m_j}{n_j}}$, $0 < p_j < q_j$, and $0 < n_j < m_j < 2n_j$; a_j, b_j are positive constants. The control laws are defined as follows,

$$\begin{cases} T_1 = -\hat{f}_1 + \ddot{\omega}_{r_{ref}} - \dot{A}_1(e_1) - \dot{B}_1(e_1) - A_2(s_1) - B_2(s_1) + u_{eq_1} \\ \dot{u}_{eq_1} = \left(-\delta_2 - |h_1| - |\dot{h}_1|\right) sign(s_2) - \alpha_1 sig^{\beta_1}(s_2) - \alpha_2 sig^{\beta_2}(s_2) \\ T_2 = -\hat{f}_2 + \dot{Q}_{s_{ref}} - A_3(e_3) - B_3(e_3) + u_{eq_2} \\ \dot{u}_{eq_2} = \left(-\delta_2 - |h_2| - |\dot{h}_2|\right) sign(s_3) - \alpha_3 sig^{\beta_1}(s_3) - \alpha_4 sig^{\beta_2}(s_3) \end{cases} \tag{46}$$

where $0 < \beta_1 < 1$ and $\beta_2 > 1$. The state observers (SO) are defined as follows,

$$\begin{cases} \dot{\hat{x}}_1 = -A_4(\tilde{x}_1) - B_4(\tilde{x}_1) + \hat{x}_{eq_1} \\ \dot{\hat{x}}_2 = \hat{f}_1 + T_1 \\ \dot{\hat{x}}_3 = \hat{f}_2 + T_2 - A_5(\tilde{x}_3) - B_5(\tilde{x}_3) + \hat{x}_{eq_2} \\ \hat{x}_{eq_1} = \left(-\eta_2 - \delta_2 - |h_2| - |\dot{h}_2| - \alpha_7 ||\hat{x}_2| + \eta_1|^{\beta_1} - \alpha_8 ||\hat{x}_2| + \eta_1|^{\beta_2}\right) sign(\sigma_1) \\ \qquad\quad -\alpha_5 sig^{\beta_1}(\sigma_1) - \alpha_6 sig^{\beta_2}(\sigma_1) \\ \hat{x}_{eq_2} = (-\delta_1 - |h_1|) sign(\sigma_2) - \alpha_9 sig^{\beta_1}(\sigma_2) - \alpha_{10} sig^{\beta_2}(\sigma_2) \end{cases} \tag{47}$$

where $\alpha_i, i = (1, 2, 3, 4, 5, 6, 7, 8, 9, 10)$ are positive constants. The disturbance observers (DO) are defined as follows,

$$\begin{cases} \hat{D}_1 = \dot{h}_1 = -A_6(Z_1) - B_6(Z_1) + \dot{q}_1 + h_{eq_1} \\ h_{eq_1} = -\alpha_{11} sig^{\beta_1}(\xi_1) - \alpha_{12} sig^{\beta_2}(\xi_1) \end{cases} \tag{48}$$

Also, we have,

$$\begin{cases} \hat{D}_2 = \dot{h}_2 = -A_7(Z_2) - B_7(Z_2) + \dot{q}_2 + h_{eq_2} \\ h_{eq_2} = -\alpha_{13} sig^{\beta_1}(\xi_2) - \alpha_{14} sig^{\beta_2}(\xi_2) \end{cases} \tag{49}$$

where $\alpha_{11}, \alpha_{12}, \alpha_{13}$, and α_{14} are positive constants.

Theorem 1. Let system (21) satisfy Assumptions 1, 2, and 3. Consider the sliding surfaces (45), control law (46), state observer (47), and disturbance observer (48) and (49). The MPPT goal is achieved in fixed time by applying the control voltages given by (26) and (27) and using (46). In the meanwhile, the convergence of the estimated data to the actual data of the system states are ensured using the SO (47) in fixed time while only the measurement of the reactive power and rotor speed are available. Also, the external disturbances and modelling uncertainties are estimated using the DO (48) and (49) and the estimated data are provided in the controller.

Proof. To obtain the fixed-time stability analysis utilizing the FOSMC method, two following phases must be considered. So, we have

Phase 1 (reaching phase). Consider the following candidate Lyapunov function that satisfies the conditions given in Lemma 3, we have

$$V = |s_2| + |s_3| + |\sigma_1| + |\sigma_2| + |\tilde{x}_2| + |\xi_1| + |\xi_2| \tag{50}$$

Taking time derivative of the candidate function yields

$$\dot{V} = \dot{s}_2 sign(s_2) + \dot{s}_3 sign(s_3) + \dot{\sigma}_1 sign(\sigma_1) + \dot{\sigma}_2 sign(\sigma_2) + \dot{\tilde{x}}_2 sign(\tilde{x}_2) + \dot{\xi}_1 sign(\xi_1) + \dot{\xi}_2 sign(\xi_2) \tag{51}$$

Before proceeding further, we need to obtain the time derivative of s_2, s_3, σ_1, σ_2, $\tilde{x}_2$, ξ_1, and ξ_2, to substitute it into (51); hence, we have

$$s_2 = \dot{s}_1 + A_2(s_1) + B_2(s_1) \xrightarrow{\dot{s}_1 = \dot{e}_2 + \dot{A}_1(e_1) + \dot{B}_1(e_1)}$$

$$s_2 = \dot{e}_2 + \dot{A}_1(e_1) + \dot{B}_1(e_1) + A_2(s_1) + B_2(s_1) \xrightarrow{\dot{e}_2 = f_1 + T_1 + d_1(t) + \Psi_1(x_1,x_2,x_3) - \ddot{\omega}_{r_{ref}}}$$

$$s_2 = f_1 + T_1 + d_1(t) + \Psi_1(x_1,x_2,x_3) - \ddot{\omega}_{r_{ref}} + \dot{A}_1(e_1) + \dot{B}_1(e_1) + A_2(s_1) + B_2(s_1) \tag{52}$$

Substituting (46) into (52) and then taking its time derivative, one can obtain

$$\dot{s}_2 = \dot{f}_1 - \dot{\hat{f}}_1 + \dot{d}_1(t) + \dot{\Psi}_1(x_1,x_2,x_3) + \left(-\delta_2 - |h_1| - |\dot{h}_1|\right)sign(s_2) - \alpha_1 sig^{\beta_1}(s_2) - \alpha_2 sig^{\beta_2}(s_2) \tag{53}$$

Similarly, using (21) and (46) and then taking its time derivative yields

$$\dot{s}_3 = \dot{f}_2 - \dot{\hat{f}}_2 + \dot{d}_2(t) + \dot{\Psi}_2(x_1,x_2,x_3) + \left(-\delta_2 - |h_2| - |\dot{h}_2|\right)sign(s_3) - \alpha_3 sig^{\beta_1}(s_3) - \alpha_4 sig^{\beta_2}(s_3) \tag{54}$$

For σ_1, we have

$$\sigma_1 = \dot{\tilde{x}}_1 + A_4(\tilde{x}_1) + B_4(\tilde{x}_1) \xrightarrow{\dot{\tilde{x}}_1 = \dot{\hat{x}}_1 - \dot{x}_1} \sigma_1 = \dot{\hat{x}}_1 - \dot{x}_1 + A_4(\tilde{x}_1) + B_4(\tilde{x}_1) \tag{55}$$

Substituting (47) into (55) and then taking its time derivative, we obtain

$$\dot{\sigma}_1 = -\dot{x}_2 + \left(-\eta_2 - \delta_2 - |h_2| - |\dot{h}_2| - \alpha_7 ||\hat{x}_2| + \eta_1|^{\beta_1} - \alpha_8 ||\hat{x}_2| + \eta_1|^{\beta_2}\right)sign(\sigma_1) - \alpha_5 sig^{\beta_1}(\sigma_1) - \alpha_6 sig^{\beta_2}(\sigma_1) \tag{56}$$

Similarly, using $\dot{\tilde{x}}_3 = \dot{\hat{x}}_3 - \dot{x}_3$ and (47) and then taking its time derivative yields

$$\dot{\sigma}_2 = \dot{f}_2 - \dot{\hat{f}}_2 + \dot{d}_2(t) + \dot{\Psi}_2(x_1,x_2,x_3) + (-\delta_1 - |h_1|)sign(\sigma_2) - \alpha_9 sig^{\beta_1}(\sigma_2) - \alpha_{10} sig^{\beta_2}(\sigma_2) \tag{57}$$

For $\tilde{x}_2$, we have

$$\dot{\tilde{x}}_2 = \dot{\hat{x}}_2 - \dot{x}_2 \xrightarrow{\dot{x}_2 = f_1 + T_1 + d_1(t) + \Psi_1(x_1,x_2,x_3) \text{ and } \dot{\hat{x}}_2 = \hat{f}_1 + T_1} \dot{\tilde{x}}_2 = -f_1 + \hat{f}_1 + d_1(t) + \Psi_1(x_1,x_2,x_3) \tag{58}$$

Also, we obtain

$$\dot{\xi}_1 = \dot{Z}_1 + A_6(Z_1) + B_6(Z_1) \xrightarrow{\dot{Z}_1 = \dot{h}_1 - \dot{q}_1} \dot{\xi}_1 = \dot{h}_1 - \dot{q}_1 + A_6(Z_1) + B_6(Z_1) \xrightarrow{\dot{h}_1 = -A_6(Z_1) - B_6(Z_1) + \dot{q}_1 + h_{eq_1}} \dot{\xi}_1 = -\alpha_{11} sig^{\beta_1}(\xi_1) - \alpha_{12} sig^{\beta_2}(\xi_1) \tag{59}$$

Similarly, using (44) and (49), we have

$$\dot{\xi}_2 = -\alpha_{13} sig^{\beta_1}(\xi_2) - \alpha_{14} sig^{\beta_2}(\xi_2) \tag{60}$$

Now substituting (53), (54), (56), (57), (58), (59), (60) into (51), yields

$$\dot{V} = \left(\dot{f}_1 - \dot{\hat{f}}_1 + \dot{d}_1(t) + \dot{\Psi}_1(x_1,x_2,x_3) + \left(-\delta_2 - |h_1| - |\dot{h}_1|\right)sign(s_2) - \alpha_1 sig^{\beta_1}(s_2) -$$

$$\alpha_2 sig^{\beta_2}(s_2)\right)sign(s_2) + \left(\dot{f}_2 - \dot{\hat{f}}_2 + \dot{d}_2(t) + \dot{\Psi}_2(x_1,x_2,x_3) + \left(-\delta_2 - |h_2| - |\dot{h}_2|\right)sign(s_3) - \alpha_3 sig^{\beta_1}(s_3) -$$

$$\alpha_4 sig^{\beta_2}(s_3)\right)sign(s_3) + \left(-\dot{x}_2 + \left(-\eta_2 - \delta_2 - |h_2| - |\dot{h}_2| - \alpha_7 ||\hat{x}_2| + \eta_1|^{\beta_1} - \alpha_8 ||\hat{x}_2| + \eta_1|^{\beta_2}\right)sign(\sigma_1) -$$

$$\alpha_5 sig^{\beta_1}(\sigma_1) - \alpha_6 sig^{\beta_2}(\sigma_1)\right)sign(\sigma_1) + \left(\dot{f}_2 - \dot{\hat{f}}_2 + \dot{d}_2(t) + \dot{\Psi}_2(x_1,x_2,x_3) + (-\delta_1 - |h_1|)sign(\sigma_2) -$$

$$\alpha_9 sig^{\beta_1}(\sigma_2) - \alpha_{10} sig^{\beta_2}(\sigma_2)\right)sign(\sigma_2) + \left(-f_1 + \hat{f}_1 + d_1(t) + \Psi_1(x_1,x_2,x_3)\right)sign(\tilde{x}_2) + \left(-\alpha_{11} sig^{\beta_1}(\xi_1) -$$

$$\alpha_{12} sig^{\beta_2}(\xi_1)\right)sign(\xi_1) + \left(-\alpha_{13} sig^{\beta_1}(\xi_2) - \alpha_{14} sig^{\beta_2}(\xi_2)\right)sign(\xi_2) \tag{61}$$

Simplifying (61) and using Definition 1 and 2 in Subsection 3.2.1 as well as $D_1 = d_1(t) + \Psi_1(x_1,x_2,x_3)$, $D_2 = d_2(t) + \Psi_2(x_1,x_2,x_3)$, we have

$$\dot{V} \le \left|\dot{f}_1 - \dot{\hat{f}}_1\right| + |\dot{D}_1| - \delta_2 - |h_1| - |\dot{h}_1| - \alpha_1 |s_2|^{\beta_1} - \alpha_2 |s_2|^{\beta_2} + \left|\dot{f}_2 - \dot{\hat{f}}_2\right| + |\dot{D}_2| - \delta_2 - |h_2| - |\dot{h}_2| -$$

$$\alpha_3 |s_3|^{\beta_1} - \alpha_4 |s_3|^{\beta_2} + |\dot{x}_2| - \eta_2 - \delta_2 - |h_2| - |\dot{h}_2| - \alpha_7 ||\hat{x}_2| + \eta_1|^{\beta_1} - \alpha_8 ||\hat{x}_2| + \eta_1|^{\beta_2} - \alpha_5 |\sigma_1|^{\beta_1} - \alpha_6 |\sigma_1|^{\beta_2} +$$

$$\left|\dot{f}_2 - \dot{\hat{f}}_2\right| + \left|\dot{D}_2\right| - \delta_1 - |h_1| - \alpha_9|\sigma_2|^{\beta_1} - \alpha_{10}|\sigma_2|^{\beta_2} + \left|\hat{f}_1 - f_1\right| + |D_1| - \alpha_{11}|\xi_1|^{\beta_1} - \alpha_{12}|\xi_1|^{\beta_2} - \alpha_{13}|\xi_2|^{\beta_1} -$$
$$\alpha_{14}|\xi_2|^{\beta_2} \tag{62}$$

Simplifying (62) and using Assumption 2 and 3 as well as $|\tilde{x}_2| \leq \left||\hat{x}_2| + \eta\right|$, we obtain

$$\dot{V} \leq -\alpha_1|s_2|^{\beta_1} - \alpha_2|s_2|^{\beta_2} - \alpha_3|s_3|^{\beta_1} - \alpha_4|s_3|^{\beta_2} - \alpha_5|\sigma_1|^{\beta_1} - \alpha_6|\sigma_1|^{\beta_2} - \alpha_7|\tilde{x}_2|^{\beta_1} - \alpha_8|\tilde{x}_2|^{\beta_2} - \alpha_9|\sigma_2|^{\beta_1} -$$
$$\alpha_{10}|\sigma_2|^{\beta_2} - \alpha_{11}|\xi_1|^{\beta_1} - \alpha_{12}|\xi_1|^{\beta_2} - \alpha_{13}|\xi_2|^{\beta_1} - \alpha_{14}|\xi_2|^{\beta_2} \tag{63}$$

Considering $\Delta_1 = min(\alpha_1, \alpha_3, \alpha_5, \alpha_7, \alpha_9, \alpha_{11}, \alpha_{13})$ and $\Delta_2 = mi\,n(\alpha_2, \alpha_4, \alpha_6, \alpha_8, \alpha_{10}, \alpha_{12}, \alpha_{14})$, we have

$$\dot{V} \leq -\Delta_1\left(|s_2|^{\beta_1} + |s_3|^{\beta_1} + |\sigma_1|^{\beta_1} + |\tilde{x}_2|^{\beta_1} + |\sigma_2|^{\beta_1} + |\xi_1|^{\beta_1} + |\xi_2|^{\beta_1}\right) - \Delta_2\left(|s_2|^{\beta_2} + |s_3|^{\beta_2} + |\sigma_1|^{\beta_2} + |\tilde{x}_2|^{\beta_2} + |\sigma_2|^{\beta_2} + |\xi_1|^{\beta_2} + |\xi_2|^{\beta_2}\right) \tag{64}$$

According to Lemma 1 and 2, we obtain

$$\dot{V} \leq -\Delta_1(|s_2| + |s_3| + |\sigma_1| + |\sigma_2| + |\tilde{x}_2| + |\xi_1| + |\xi_2|)^{\beta_1} - \Delta_2 7^{1-\beta_2}(|s_2| + |s_3| + |\sigma_1| + |\sigma_2| + |\tilde{x}_2| + |\xi_1| +$$
$$|\xi_2|)^{\beta_2} \quad ➜ \quad \dot{V} \leq -\Delta_1(V)^{\beta_1} - \Delta_2 7^{1-\beta_2}(V)^{\beta_2} \tag{65}$$

Considering $\rho_1 = \Delta_1, \rho_2 = \beta_1, \rho_3 = \Delta_2 7^{1-\beta_2}$, and $\rho_4 = \beta_2$, yields

$$\dot{V} \leq -\rho_1 V^{\rho_2} - \rho_3 V^{\rho_4} \tag{66}$$

Thus, according to lemma 3, we have $\rho_1, \rho_3 > 0, 0 < \rho_2 < 1$, and $\rho_4 > 1$; hence, we obtain $\Delta_1 > 0, \Delta_2 7^{1-\beta_2} > 0$, $0 < \beta_1 < 1$, and $\beta_2 > 1$. Also, we have $s_2 \to 0$, $s_3 \to 0$ $\tilde{x}_2 \to 0$, $\sigma_1 \to 0$, $\sigma_2 \to 0$, $\xi_1 \to 0$ and $\xi_2 \to 0$ within fixed time given as follows

$$T_1 \leq \frac{1}{\rho_1(1-\rho_2)} + \frac{1}{\rho_3(\rho_4-1)} \tag{67}$$

Therefore, the proof of reaching phase is completed.

Phase 2 (sliding phase). Based on Lemma 4 and the definition of errors in this section, we have

$$\begin{cases} \dot{s}_1 = -A_2(s_1) - B_2(s_1) \\ \dot{e}_3 = -A_3(e_3) - B_3(e_3) \\ \dot{\tilde{x}}_1 = -A_4(\tilde{x}_1) - B_4(\tilde{x}_1) \\ \dot{\tilde{x}}_3 = -(\tilde{x}_3) - B_5(\tilde{x}_3) \\ Z_1 = -\int A_6(Z_1)dt - \int B_6(Z_1)dt \\ Z_2 = -\int A_7(Z_2)dt - \int B_7(Z_2)dt \end{cases} \quad ➜$$

$$\begin{cases} \tilde{x}_2 \to 0 \Rightarrow \hat{x}_2 \to x_2 \\ \dot{s}_1 = -A_2(s_1) - B_2(s_1) \Rightarrow s_1 \to 0 \Rightarrow \dot{e}_1 = -A_1(e_1) - B_1(e_1) \Rightarrow e_1 \to 0 \; \dot{e}_1 = e_2 \to 0 \\ \dot{e}_3 = -A_3(e_3) - B_3(e_3) \Rightarrow e_3 \to 0 \\ \dot{\tilde{x}}_1 = -A_4(\tilde{x}_1) - B_4(\tilde{x}_1) \Rightarrow \tilde{x}_1 \to 0 \Rightarrow \hat{x}_1 \to x_1 \\ \dot{\tilde{x}}_3 = -(\tilde{x}_3) - B_5(\tilde{x}_3) \Rightarrow \tilde{x}_3 \to 0 \Rightarrow \hat{x}_3 \to x_3 \\ \dot{Z}_1 = -A_6(Z_1) - B_6(Z_1) \Rightarrow Z_1 \to 0 \Rightarrow \widehat{D}_1 \to D_1 \\ \dot{Z}_2 = -A_7(Z_2) - B_7(Z_2) \Rightarrow Z_2 \to 0 \Rightarrow \widehat{D}_2 \to D_2 \end{cases} \tag{68}$$

Hence, the sliding phase is completed within fixed time given as

$$T_2 \leq \sum_{j=1}^{4} \frac{1}{a_j} \frac{m_j}{m_j - n_j} + \frac{1}{b_j} \frac{q_j}{q_j - p_j} \tag{69}$$

Finally, we have $T = T_1 + T_2$; where T is the total convergence time. This concludes the proof. ∎

Proposition 1. Let system (21) satisfy Assumptions 1, 2, and 3. Consider the sliding surfaces (70), control law (71), state observer (72), and disturbance observer (73) and (74). The MPPT goal is achieved in finite time by applying the control voltages given by (26) and (27) and using (71). In the meanwhile, the convergence of the estimated data to the actual data of the system states are ensured using the SO (72) in finite time while only the measurement of the reactive power and rotor speed are available. Also, the external disturbances and modelling uncertainties are estimated using the DO (73) and (74) and the estimated data are provided in the controller.

$$\begin{cases} s_1 = \dot{e}_1 + A_1(e_1) \\ s_2 = \dot{s}_1 + A_2(s_1) \\ s_3 = \dot{e}_3 + A_3(e_3) \\ \sigma_1 = \dot{\tilde{x}}_1 + A_4(\tilde{x}_1) \\ \sigma_2 = \dot{\tilde{x}}_3 + A_5(\tilde{x}_3) \\ \xi_1 = Z_1 + \int A_6(Z_1)dt \\ \xi_2 = Z_2 + \int A_7(Z_2)dt \end{cases} \tag{70}$$

where we have $A_j(\varrho) = a_j \varrho^{\frac{p_j}{q_j}}; 0 < p_j < q_j; a_j$ is positive constant.

$$\begin{cases} T_1 = -\hat{f}_1 + \ddot{\omega}_{r_{ref}} - \dot{A}_1(e_1) - A_2(s_1) + u_{eq_1} \\ \dot{u}_{eq_1} = (-\delta_2 - |h_1| - |\dot{h}_1|)sign(s_2) - \alpha_1 sig^{\beta_1}(s_2) \\ T_2 = -\hat{f}_2 + \dot{Q}_{s_{ref}} - A_3(e_3) + u_{eq_2} \\ \dot{u}_{eq_2} = (-\delta_2 - |h_2| - |\dot{h}_2|)sign(s_3) - \alpha_2 sig^{\beta_1}(s_3) \end{cases} \tag{71}$$

where $0 < \beta_1 < 1$. The state observer (SO) is defined as follows,

$$\begin{cases} \dot{\hat{x}}_1 = -A_4(\tilde{x}_1) + \hat{x}_{eq_1} \\ \dot{\hat{x}}_2 = \hat{f}_1 + T_1 \\ \dot{\hat{x}}_3 = \hat{f}_2 + T_2 - A_5(\tilde{x}_3) + \hat{x}_{eq_2} \\ \dot{\hat{x}}_{eq_1} = \left(-\eta_2 - \delta_2 - |h_2| - |\dot{h}_2| - \alpha_4 ||\hat{x}_2| + \eta_1|^{\beta_1}\right) sign(\sigma_1) - \alpha_3 sig^{\beta_1}(\sigma_1) \\ \dot{\hat{x}}_{eq_2} = (-\delta_1 - |h_1|)sign(\sigma_2) - \alpha_5 sig^{\beta_1}(\sigma_2) \end{cases} \tag{72}$$

where $\alpha_i, i = (1,2,3,4,5)$ are positive constants. The disturbance observer (DO) is defined as follows,

$$\begin{cases} \hat{D}_1 = \dot{h}_1 = -A_6(Z_1) + \dot{q}_1 + h_{eq_1} \\ h_{eq_1} = -\alpha_6 sig^{\beta_1}(\xi_1) \end{cases} \tag{73}$$

Also, we have,

$$\begin{cases} \hat{D}_2 = \dot{h}_2 = -A_7(Z_2) + \dot{q}_2 + h_{eq_2} \\ h_{eq_2} = -\alpha_7 sig^{\beta_1}(\xi_2) \end{cases} \tag{74}$$

where α_6 and α_7 are positive constants.

Remark 2. It should be noted that the idea behind the design of the SMC law of the finite-time method (given in Proposition 1) is similar to the one given in [68] that is incorporated with our proposed state and disturbance observers.

4. Simulation results

In this section, the applicability and validity of the fixed-time observer-based controller design is tested for MPPT of a grid-connected DFIG based WECS (given in [7, 68, 87, 90] and described in Section 3). The proposed fixed-time method (FOSMC) in this research is also compared with a finite-time observer-based controller (given in Proposition 1) to show its effectiveness in improving overall tracking performance than a classical method. The simulation has been executed on Simulink/MATLAB by utilizing the solver of 'ode1be' and the step-size of 0.01. The design parameters for both control methods (i.e., the proposed fixed-time method and the finite-time method) are considered the same to make a reasonable comparison among the simulation results.

The simulation has been done in two different scenarios of wind speed modelling: Scenario 1) Step change of the wind speed and Scenario; 2) Random variation of the wind speed. Note that in both scenarios (and both control methods), the wind velocity is considered to be below the rated value; i.e., the considered wind speed is from $8(m/s)$ to $12(m/s)$. The considered design parameters for Scenarios 1 and 2 and for both control methods are given in Table 2. Also, the system parameters have been given in [1, 10, 27, 52] and in Section 3. The system initial conditions are considered as: $x_1(0) = 0.1$, $x_2(0) = 0$, $x_3(0) = 0.01$. The models of the disturbances, $d_1(t)$ and $d_2(t)$, are considered for both scenarios as: $d_{1,2}(t) = 0.01 \sin(t)$, which is added to the system at $t = 8(s)$. The modelling uncertainties, $\Psi_1(x_1, x_2, x_3)$ and $\Psi_2(x_1, x_2, x_3)$, are considered as: $\Psi_{1,2}(x_1, x_2, x_3) = 0.014 \sin(x1) -$

$0.013 \cos(x2) - 0.013 \sin(x3)$. Then, the sum of modelling uncertainties and external disturbances of the system are defined as: $D_1 = d_1(t) + \Psi_1(x_1, x_2, x_3)$ and $D_2 = d_2(t) + \Psi_2(x_1, x_2, x_3)$ that is estimated by DO.

Table 2. The considered design parameters for the simulation.

	δ_1	δ_2	η_1	η_2	p_j/q_j	m_j/n_j	β_1	β_2
Scenario 1	0.2	0.01	0.06	0.001	101/103	105/103	101/103	105/103
Scenario 2	0.1	0.1	0.6	0.01	101/103	105/103	101/103	105/103

	a_1, b_1	a_2, b_2	a_3, b_3	a_4, b_4	a_5, b_5	a_6, b_6	a_7, b_7
Scenario 1	11	11	21	7	7	10	10
Scenario 2	7	10	5	10	10	0.5	1

	α_1	α_2	α_3	α_4	α_5	α_6	α_7	α_8	α_9	α_{10}	α_{11}	α_{12}	α_{13}	α_{14}
Scenario 1	11	11	5	5	8.5	8.5	8.5	8.5	5.6	5.6	1	1	1	1
Scenario 2	15	15	10	10	10	10	10	10	10	10	1	1	1	1

Remark 3. The designer can adjust these arbitrary design parameters (given in Table 2) based on their control goals. The system's fixed settling time and control effort can be adjusted by choosing them properly. More importantly, the adjustable convergence time can be determined a priori utilizing design parameters irrespective of initial conditions using the notion of the fixed-time stability.

Remark 4. The design parameters (given in Table 2) are chosen in this paper through successive improvements to ensure a satisfactory control and observer performances and speed up the convergence rate with minimum energy consumption. For instance, controller/observer gains are chosen to ensure a proper trade-off between the convergence rates and errors; i.e., greater controller/observer gains usually provide faster convergence rates and higher tracking/estimation errors, vice versa. In addition, there are required conditions that must be considered to select these design parameters as follows:

- To avoid singularity issue, p_j, q_j, m_j, and n_j must be selected from odd numbers.
- There are the following required conditions for the design parameters in SMC laws: $0 < \beta_1 < 1; \beta_2 > 1; 0 < p_j < q_j; 0 < n_j < m_j < 2n_j$.
- Table 3 provides the controller gains and observer gains of the proposed method with their required conditions.

Table 3. Introducing the design parameters and their required conditions.

FOSMC method	Parameters	Requirements
Controller gains	$a_1, b_1, a_2, b_2, a_3, b_3, \alpha_1, \alpha_2, \alpha_3, \alpha_4$	$a_j > 0, b_j > 0, \alpha_i > 0$
State observer gains	$a_4, b_4, a_5, b_5, \alpha_5, \alpha_6, \alpha_7, \alpha_8, \alpha_9, \alpha_{10}$	$a_j > 0, b_j > 0, \alpha_i > 0$
Disturbance observer gains	$a_6, b_6, a_7, b_7, \alpha_{11}, \alpha_{12}, \alpha_{13}, \alpha_{14}$	$a_j > 0, b_j > 0, \alpha_i > 0$

The following performance criteria (given in [57]) are used in both scenarios for both control methods to provide a numerical comparison among the simulation results of the proposed fixed-time method and the finite-time method (given in Proposition 1).

I. Integral of the square value (ISV) of the control input

$$ISV_u = \int_0^{t_f} u^2 \, dt \tag{75}$$

II. Integral of the absolute value of the error (IAE)

$$IAE_{e_i} = \int_0^{t_f} |e_i| \, dt \tag{76}$$

III. Integral of the time multiplied by the absolute value of the error (ITAE)

$$ITAE_{e_i} = \int_0^{t_f} t |e_i| \, dt \tag{77}$$

where t_f is the total running time. The ITAE and IAE present the numerical measures of tracking performance for a whole error curve. The IAE gives an intermediate result, while time is as a term in ITAE that deeply emphasises the errors that occur late in time. The energy consumption can be compared using ISV criterion.

4.1. Scenario 1) step change of the wind speed

Figs. 5 to 9 display the simulation results for the first scenario. Fig. 5 (a) shows the simulation model of the wind speed in this scenario, that is, step changes of wind speed. In this scenario, wind speed changes as a series of four consecutive steps from $8(m/s)$ to $12(m/s)$ to briefly mimic a gust [27]. Fig. 5 (b), (c), and (d) shows the control performance and the SO estimation performance for the system states using the proposed fixed-time method (FOSMC). In Fig. 5 (b), the estimated data of the generator rotor speed ($\hat{\omega}_r$) reaches the actual data (ω_r) and they converge to the reference ($\omega_{r_{ref}}$). Fig. 5 (c) shows that the observed data ($\hat{\dot{\omega}}_r$) converges to the actual data ($\dot{\omega}_r$) and they reach the desired value ($\dot{\omega}_{r_d}$). In Fig. 5 (d), the convergence of the estimated data of the stator reactive power ($\hat{Q}_s$) to the actual data (Q_s) is shown as well as their convergences to the reference ($Q_{s_{ref}}$). As we can observe from Fig. 5 (b), (c), and (d), the observed data of the system states quickly follow the actual data as well as their convergences to their references are realized in a very short time with a reasonable performance and small oscillations using the proposed FOSMC.
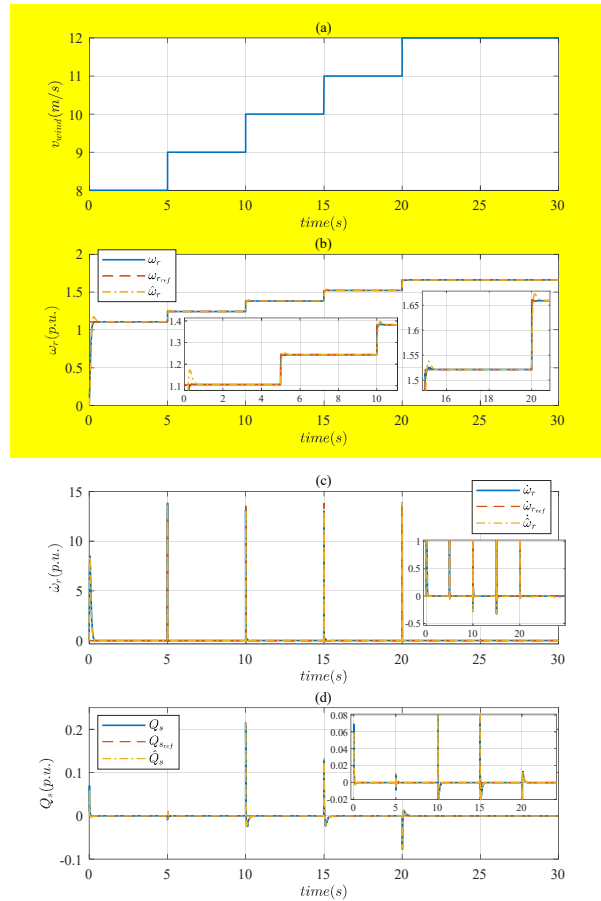

Fig. 5. (a) The considered step change of wind speed; (b), (c), and (d) The tracking performance of the system states to their references as well as the estimation performance of the system states.

Fig. 6 shows the tracking errors of the system states to their references using the proposed fixed-time method and the finite-time method. As shown in Fig. 6 (a), (b), and (c), the fixed-time method provides a faster convergence rate with a less undershoot/overshoot compared to the finite-time method. Fig. 7 (a) illustrates that the MPPT control is realized, and the power coefficient reaches to its maximum value using both methods. Fig. 7 (b) shows the convergence of the active output power to its reference (that is $P_{m_{max}}$, the maximum possible power to extract). It can be seen from Fig. 7 (a) and (b), the fixed-time method provides a faster convergence rate with less oscillations compared to the finite-time method.
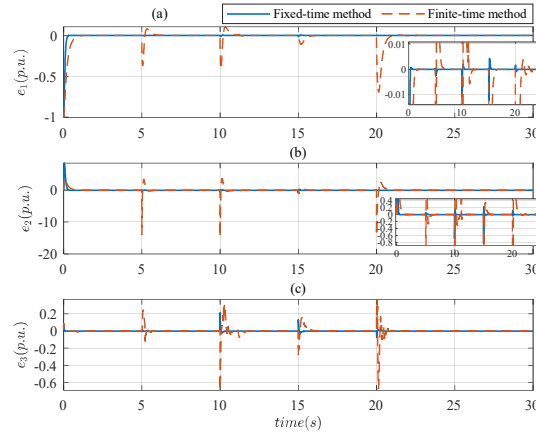
Fig. 6. The system tracking errors (a) $e_1 = \omega_r - \omega_{r_{ref}}$, (b) $e_2 = \dot{\omega}_r - \dot{\omega}_{r_{ref}}$, (c) $e_3 = Q_s - Q_{s_{ref}}$.
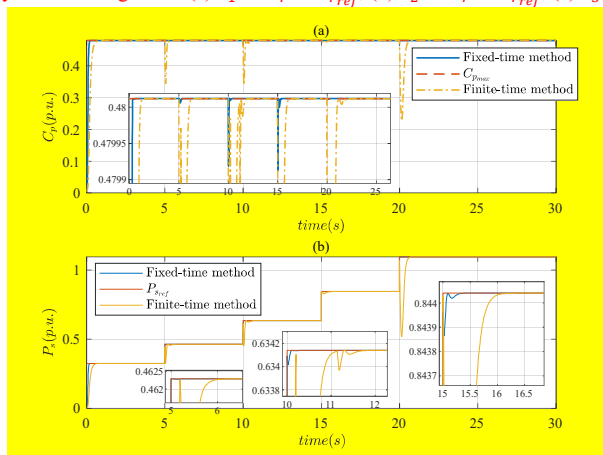

Fig. 7. (a) The tracking performance of the power coefficient to its maximum value. (b) The tracking performance of the active output power to its reference (i.e., $P_{s_{ref}} \approx P_{m_{max}}$).
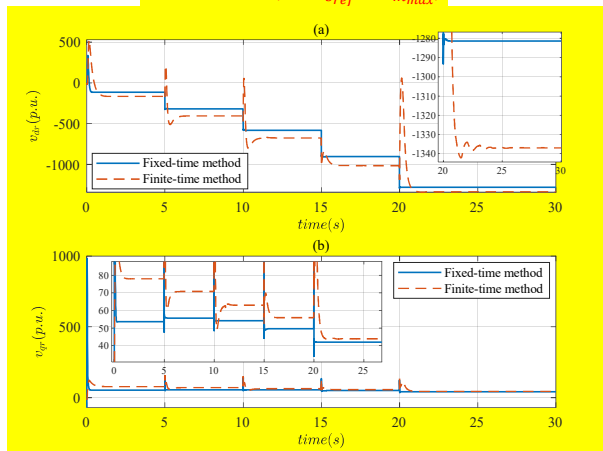

Fig. 8. The simulation waveform of the control voltages (a) v_{dr}, (b) v_{qr}.
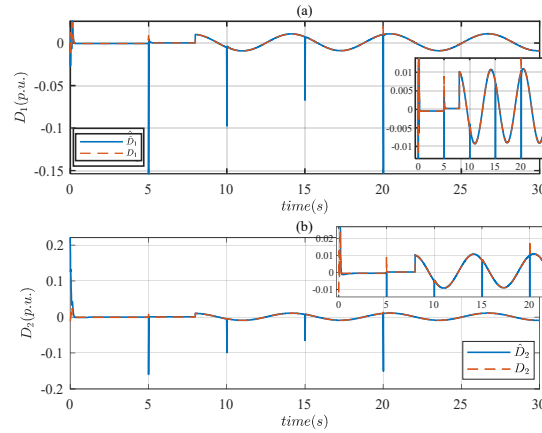
Fig. 9. The tracking performance of the estimated data to the actual data of the modelling uncertainties and external disturbances, (a) D_1, (b) D_2.

Fig. 8 (a) and (b) shows the control signals of v_{dr} and v_{qr}, respectively, for both control methods. The control voltages of the fixed-time method have less fluctuation compared to the control voltages of the finite-time method. It can be also observed that the undesirable chattering phenomenon does not exist in the control signals of both control methos. Fig. 9 (a) and (b) show the estimation performance of the modelling uncertainties and external disturbances using disturbance observer. The sum of external disturbances (added to the system at $t = 8(s)$) and modelling uncertainties are accurately estimated by DO which is fully rejected using the controller. It should be noted that the estimation of the modelling uncertainties and external disturbances are fulfilled with no information of their upper bounds in advance. In general, the fixed-time method shows a great robustness against the modelling uncertainties and external disturbances and provides faster convergence rate with a more reasonable tracking performance compared to the finite-time method.

Table 4. Comparison of the performance indices for Scenario 1.

Scenario 1	ISV_{u_1}	ISV_{u_2}	IAE_{e_1}	IAE_{e_2}	IAE_{e_3}	$ITAE_{e_1}$	$ITAE_{e_2}$	$ITAE_{e_3}$
Fixed-time	$2.2776e + 07$	$9.6334e + 04$	0.0827	1.0774	0.0213	0.0450	0.9780	0.2658
Finite-time	$2.5407e + 07$	$1.1704e + 05$	0.6738	4.6078	0.3197	6.9360	47.6338	4.3763

Table 4 provides a comparison of the performance indexes of the fixed-time method and finite-time method. It can be seen from Table 4 that the proposed fixed-time method gives lower numerical values for ISV_u, IAE_{e_i}, and $ITAE_{e_i}$ over the finite-time method. Consequently, the proposed method outperforms the other method in terms of these three performance criteria.

4.2. Scenario 2) random variation of the wind speed

Figs. 10 to 14 show the simulation results for the second scenario. Fig. 10 (a) shows the simulation model of the wind speed in this scenario, that is, random wind speed variation. In this scenario, wind speed changes stochastically that is started from $8(m/s)$ and gradually reaching $12(m/s)$ [27]. In Fig. 10 (b), (c), and (d), the control performance and the state observer performance for the system states is shown using the proposed method (FOSMC). Fig. 10 (b) shows the convergence of the estimated data of the generator rotor speed ($\hat{\omega}_r$) to the actual data (ω_r) as well as the convergence of them to the required trajectory ($\omega_{r_{ref}}$). In Fig. 10 (c), the observed data ($\hat{\dot{\omega}}_r$) converges to the actual data ($\dot{\omega}_r$) and they reach the reference ($\dot{\omega}_{r_d}$). In Fig. 10 (d), the estimated data of the stator reactive power ($\hat{Q}_s$) reaches the actual data (Q_s) and they converge to the reference ($Q_{s_{ref}}$). As shown in Fig. 10 (b), (c), and (d), the estimated data and actual data are tracked in a very short time as well as the convergence of the actual data to their required trajectories are realized in a short time with a satisfactory performance. So, the state observer and tracking controller in the presence of external disturbances (added to the system at $t = 8(s)$) and modelling uncertainties show an effective and reasonable performance thanks to the disturbance rejection.
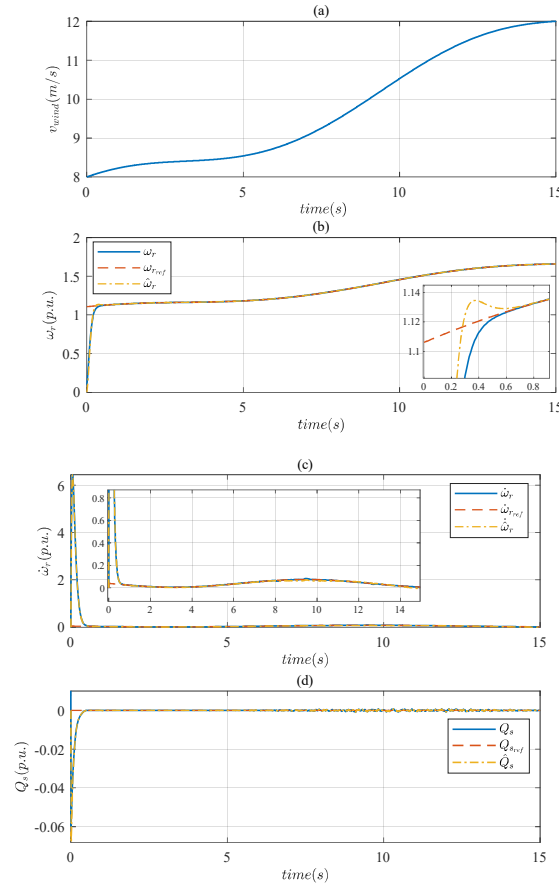
Fig. 10. (a) The considered step change of wind speed. (b), (c), and (d) The tracking performance of the system states to their references as well as the estimation performance of the system states.

In Fig. 11, the tracking errors of the system states to their required trajectories are provided utilizing the fixed-time method and the finite-time method. As we can see from Fig. 11 (a), (b), and (c), the convergence time of the proposed method is faster than the other one. Also, it can be seen from Fig. 11 (c) that the fixed-time method provides a greater robustness against the external disturbances (added to the system at $t = 8(s)$) and modelling uncertainties compared to the finite-time method. Fig. 12 (a) shows the convergence of the power coefficient to its maximum value which means the MPPT control is realized. Fig. 12 (b) shows the active output power converges to its required trajectory $P_{S_{ref}} \approx P_{m_{max}}$ (which is the maximum possible power to extract). As we can observe from Fig. 12 (a) and (b), a faster convergence time is provided using the proposed method in comparison with the finite-time method.
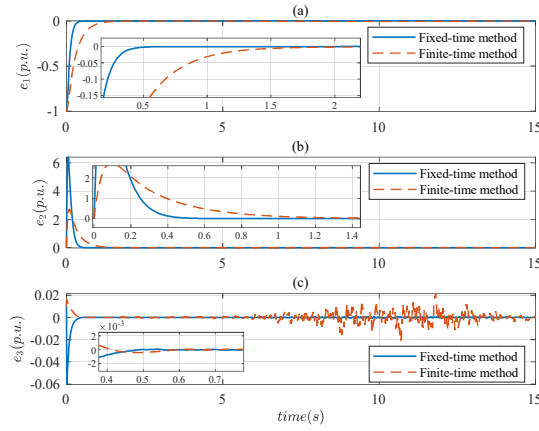
Fig. 11. The system tracking errors (a) $e_1 = \omega_r - \omega_{r_{ref}}$, (b) $e_2 = \dot{\omega}_r - \dot{\omega}_{r_{ref}}$, (c) $e_3 = Q_s - Q_{s_{ref}}$.
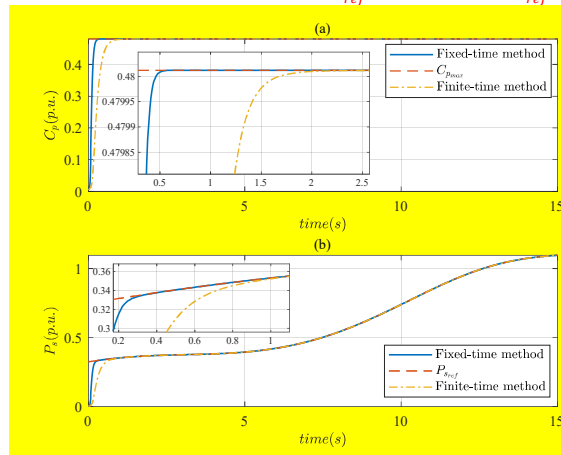

Fig. 12. (a) The tracking performance of the power coefficient to its maximum value. (b) The tracking performance of the power to its reference (i.e., $P_{s_{ref}} \approx P_{m_{max}}$).
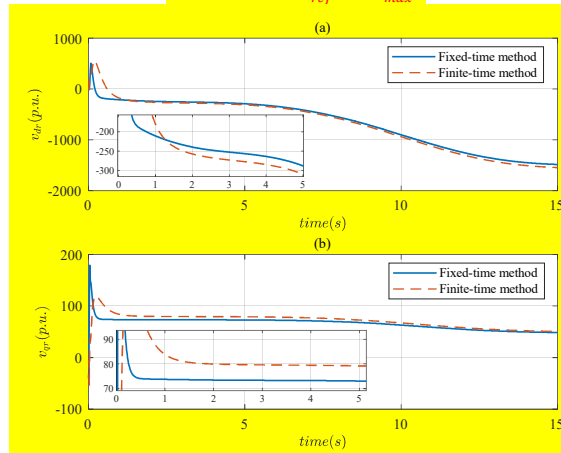

Fig. 13. The simulation waveform of the control voltages (a) v_{dr}, (b) v_{qr}.
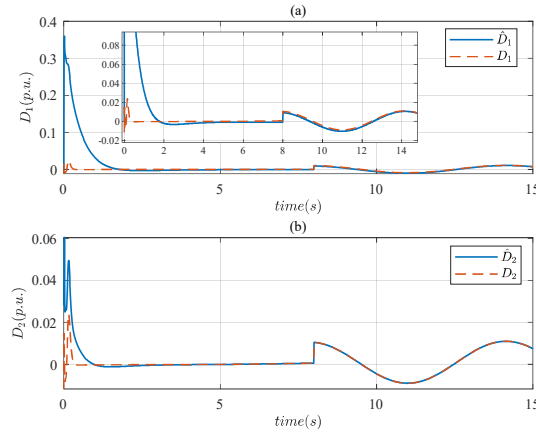
Fig. 14. The tracking performance of the estimated data to the actual data of the modelling uncertainties and external disturbances (a) D_1, (b) D_2.

In Fig. 13 (a) and (b), the signals of the control voltages v_{dr} and v_{qr} for both control methods are provided. As we can see from Fig. 13 (a) and (b), there are no chattering issue in the control signals for both control methods which shows the effectiveness of the proposed solution for removing chattering. In Fig. 14 (a) and (b), the disturbance observer performance for estimating the modelling uncertainties and external disturbances is shown. As we can see from Fig. 14, the accuracy and satisfactory performance of the proposed DO for estimating the sum of external disturbances (added to the system at $t = 8(s)$) and modelling uncertainties are demonstrated while there was no information of their upper bounds in advance. So, as this estimated data is used in the controller for disturbance rejection, a great robustness of the proposed FOSMC method is provided and proven from the results.

Table 5. Comparison of the performance indices for Scenario 2.

Scenario 2	ISV_{u_1}	ISV_{u_2}	IAE_{e_1}	IAE_{e_2}	IAE_{e_3}	$ITAE_{e_1}$	$ITAE_{e_2}$	$ITAE_{e_3}$
Fixed-time	$1.0083e + 07$	$6.8157e + 04$	0.1208	1.0135	0.0077	0.0937	0.1819	0.0194
Finite-time	$1.0980e + 07$	$7.9376e + 04$	0.3431	1.0378	0.0345	0.3965	0.6099	0.3257

Table 5 presents a comparison of the performance indexes of the two methods. The proposed fixed-time method provides lower numerical values for ISV_u, IAE_{e_i}, and $ITAE_{e_i}$ (in most cases) compared to the other method. As a result, the proposed method is better than the finite-time method in terms of these three performance criteria.

5. Conclusion

In this paper, a novel incorporation of sliding mode controller, sliding mode state and disturbance observers, and fixed-time stability notion is done to develop the FOSMC method for MPPT of DFIG based WECS. The FOSMC method is designed while only the measurement of the stator reactive power and rotor speed is needed and there is no information of the upper bounds of external disturbances and modelling uncertainties in advance. The key advantages of the proposed approach are fixed-time convergence, chattering elimination, and strong robustness to unknown disturbances and uncertainties. The stability proof is given for the closed-loop nonlinear system using the proposed observer-based controller by considering a proper Lyapunov function and considering the separation principle. The simulation results of the proposed fixed-time method and a classical finite-time method are carried out. The results of simulation and numerical comparison demonstrate that the proposed method has a satisfactory estimation and MPPT performance with a fast convergence rate and outperforms the finite-time method. For future works, a combined chattering-free robust SMC with deep learning and reinforcement learning is aimed to be developed to provide an incorporation of a conventional controller and intelligent controller for MPPT of DFIG based WECS. As for meta-parameter selection, we will set the problem up as a multi-objective constrained decision process and use a genetic algorithm to select the parameters.

6. Competing interests

The authors declare that they have no conflicts of interest.

7. References

[1]   B. Yang, X. Zhang, T. Yu, H. Shu, and Z. Fang, "Grouped grey wolf optimizer for maximum power point tracking of doubly-fed induction generator based wind turbine," *Energy conversion and management,* vol. 133, pp. 427-443, 2017.

[2]   M. M. Savino, R. Manzini, V. Della Selva, and R. Accorsi, "A new model for environmental and economic evaluation of renewable energy systems: The case of wind turbines," *Applied energy,* vol. 189, pp. 739-752, 2017.

[3]   J. Pedra, L. Sainz, and L. Monjo, "Comparison of small-signal admittance-based models of doubly-fed induction generators," *International Journal of Electrical Power & Energy Systems,* vol. 145, p. 108654, 2023.

[4]   P. Li, J. Wang, L. Xiong, S. Huang, M. Ma, and Z. Wang, "Energy-shaping controller for DFIG-based wind farm to mitigate subsynchronous control interaction," *IEEE Transactions on Power Systems,* vol. 36, no. 4, pp. 2975-2991, 2020.

[5]   P. Li, L. Xiong, F. Wu, M. Ma, and J. Wang, "Sliding mode controller based on feedback linearization for damping of sub-synchronous control interaction in DFIG-based wind power plants," *International Journal of Electrical Power & Energy Systems,* vol. 107, pp. 239-250, 2019.

[6]   D. Yang, G.-g. Yan, T. Zheng, X. Zhang, and L. Hua, "Fast Frequency Response of a DFIG Based on Variable Power Point Tracking Control," *IEEE Transactions on Industry Applications,* 2022.

[7]   S. Li, T. A. Haskew, K. A. Williams, and R. P. Swatloski, "Control of DFIG wind turbine with direct-current vector control configuration," *IEEE transactions on Sustainable Energy,* vol. 3, no. 1, pp. 1-11, 2011.

[8]   B. Bossoufi, M. Karim, A. Lagrioui, M. Taoussi, and A. Derouich, "Observer backstepping control of DFIG-Generators for wind turbines variable-speed: FPGA-based implementation," *Renewable Energy,* vol. 81, pp. 903-917, 2015.

[9]   Y. El Mourabit, A. Derouich, A. El Ghzizal, N. El Ouanjli, and O. Zamzoum, "Nonlinear backstepping control for PMSG wind turbine used on the real wind profile of the Dakhla‐Morocco city," *International Transactions on Electrical Energy Systems,* vol. 30, no. 4, p. e12297, 2020.

[10]   B. Yang, L. Jiang, L. Wang, W. Yao, and Q. Wu, "Nonlinear maximum power point tracking control and modal analysis of DFIG based wind turbine," *International Journal of Electrical Power & Energy Systems,* vol. 74, pp. 429-436, 2016.

[11]   S. Taraft, D. Rekioua, D. Aouzellag, and S. Bacha, "A proposed strategy for power optimization of a wind energy conversion system connected to the grid," *Energy Conversion and Management,* vol. 101, pp. 489-502, 2015.

[12]   J. Hu, H. Nian, B. Hu, Y. He, and Z. Zhu, "Direct active and reactive power regulation of DFIG using sliding-mode control approach," *IEEE Transactions on energy conversion,* vol. 25, no. 4, pp. 1028-1039, 2010.

[13]   C. Edwards and S. Spurgeon, *Sliding mode control: theory and applications*. Crc Press, 1998.

[14]   K. Shihabudheen, S. K. Raju, and G. Pillai, "Control for grid‐connected DFIG‐based wind energy system using adaptive neuro‐fuzzy technique," *International transactions on electrical energy systems,* vol. 28, no. 5, p. e2526, 2018.

[15]   M. Makhad, K. Zazi, M. Zazi, and A. Loulijat, "Adaptive super-twisting terminal sliding mode control and LVRT capability for switched reluctance generator based wind energy conversion system," *International Journal of Electrical Power & Energy Systems,* vol. 141, p. 108142, 2022.

[16]   L. Xiong, P. Li, F. Wu, M. Ma, M. W. Khan, and J. Wang, "A coordinated high-order sliding mode control of DFIG wind turbine for power optimization and grid synchronization," *International Journal of Electrical Power & Energy Systems,* vol. 105, pp. 679-689, 2019.

[17]   C. Zhang, S. Gutierrez, F. Plestan, and J. de León-Morales, "Adaptive super-twisting control of floating wind turbines with collective blade pitch control," *IFAC-PapersOnLine,* vol. 52, no. 4, pp. 117-122, 2019.

[18]   P. Li, J. Wang, L. Xiong, and M. Ma, "Robust nonlinear controller design for damping of sub-synchronous control interaction in DFIG-based wind farms," *IEEE Access,* vol. 7, pp. 16626-16637, 2019.

[19]   D.-y. Chen, Y.-x. Liu, X.-y. Ma, and R.-f. Zhang, "Control of a class of fractional-order chaotic systems via sliding mode," *Nonlinear Dynamics,* vol. 67, no. 1, pp. 893-901, 2012.

[20] C. Cabal, L. Martínez-Salamero, L. Séguier, C. Alonso, and F. Guinjoan, "Maximum power point tracking based on slidingmode control for output-series connected converters in photovoltaic systems," *IET Power Electronics,* vol. 7, no. 4, pp. 914-923, 2014.

[21] M. Zhihong, A. P. Paplinski, and H. R. Wu, "A robust MIMO terminal sliding mode control scheme for rigid robotic manipulators," *IEEE transactions on automatic control,* vol. 39, no. 12, pp. 2464-2469, 1994.

[22] J. Mérida, L. T. Aguilar, and J. Dávila, "Analysis and synthesis of sliding mode control for large scale variable speed wind turbine for power optimization," *Renewable Energy,* vol. 71, pp. 715-728, 2014.

[23] J. Wang, D. Bo, Q. Miao, Z. Li, X. Wu, and D. Lv, "Maximum power point tracking control for a doubly fed induction generator wind energy conversion system based on multivariable adaptive super-twisting approach," *International Journal of Electrical Power & Energy Systems,* vol. 124, p. 106347, 2021.

[24] A. Polyakov, "Nonlinear feedback design for fixed-time stabilization of linear control systems," *IEEE Transactions on Automatic Control,* vol. 57, no. 8, pp. 2106-2110, 2011.

[25] P. A. Hosseinabadi, A. S. S. Abadi, S. Mekhilef, and H. R. Pota, "Fixed-Time Adaptive Robust Synchronization with a State Observer of Chaotic Support Structures for Offshore Wind Turbines," *Journal of Control, Automation and Electrical Systems,* vol. 32, no. 4, pp. 942-955, 2021.

[26] A. Tohidi, H. Hajieghrary, and M. A. Hsieh, "Adaptive disturbance rejection control scheme for DFIG-based wind turbine: Theory and experiments," *IEEE Transactions on Industry Applications,* vol. 52, no. 3, pp. 2006-2015, 2016.

[27] B. Yang, T. Yu, H. Shu, J. Dong, and L. Jiang, "Robust sliding-mode control of wind energy conversion systems for optimal power extraction via nonlinear perturbation observers," *Applied Energy,* vol. 210, pp. 711-723, 2018.

[28] G. Rigatos, P. Siano, N. Zervos, and C. Cecati, "Control and disturbances compensation for doubly fed induction generators using the derivative-free nonlinear Kalman filter," *IEEE Transactions on Power Electronics,* vol. 30, no. 10, pp. 5532-5547, 2014.

[29] B. Yang, L. Jiang, W. Yao, and Q. Wu, "Perturbation estimation based coordinated adaptive passive control for multimachine power systems," *Control Engineering Practice,* vol. 44, pp. 172-192, 2015.

[30] J. P. Gauthier, H. Hammouri, and S. Othman, "A simple observer for nonlinear systems applications to bioreactors," *IEEE Transactions on automatic control,* vol. 37, no. 6, pp. 875-880, 1992.

[31] M. Hou and P. Muller, "Design of observers for linear systems with unknown inputs," *IEEE Transactions on automatic control,* vol. 37, no. 6, pp. 871-875, 1992.

[32] P. Moraal and J. Grizzle, "Observer design for nonlinear systems with discrete-time measurements," *IEEE Transactions on automatic control,* vol. 40, no. 3, pp. 395-404, 1995.

[33] H. Zhang and J. Wang, "Adaptive sliding-mode observer design for a selective catalytic reduction system of ground-vehicle diesel engines," *IEEE/ASME Transactions on Mechatronics,* vol. 21, no. 4, pp. 2027-2038, 2016.

[34] S. Mascolo and G. Grassi, "Controlling chaos via backstepping design," *Physical Review E,* vol. 56, no. 5, p. 6166, 1997.

[35] A. Fradkov, H. Nijmeijer, and A. Markov, "Adaptive observer-based synchronization for communication," *International Journal of Bifurcation and Chaos,* vol. 10, no. 12, pp. 2807-2813, 2000.

[36] D. López-Mancilla, C. Cruz-Hernández, and C. Posadas-Castillo, "A modified chaos-based communication scheme using Hamiltonian forms and observer," in *Journal of Physics: Conference Series*, 2005, vol. 23, no. 1, p. 267: IOP Publishing.

[37] T. L. Carroll and L. M. Pecora, "Synchronizing chaotic circuits," *IEEE Transactions on circuits and systems,* vol. 38, no. 4, pp. 453-456, 1991.

[38] G. Grassi and S. Mascolo, "Nonlinear observer design to synchronize hyperchaotic systems via a scalar signal," *IEEE Transactions on Circuits and Systems I: Fundamental Theory and Applications,* vol. 44, no. 10, pp. 1011-1014, 1997.

[39] M. Arcak and P. Kokotović, "Nonlinear observers: a circle criterion design and robustness analysis," *Automatica,* vol. 37, no. 12, pp. 1923-1930, 2001.

[40] Y. Huangfu, J. Xu, S. Zhuo, M. Xie, and Y. Liu, "A novel adaptive sliding mode observer for SOC estimation of lithium batteries in electric vehicles," in *Power Electronics Systems and Applications-Smart Mobility, Power Transfer & Security (PESA), 2017 7th International Conference on*, 2017, pp. 1-6: IEEE.

[41]   Y. Sang, B. Yang, W. Yao, and L. Jiang, "Design and implementation of perturbation observer‐based robust passivity‐based control for VSC‐MTDC systems considering offshore wind power integration," *IET Generation, Transmission & Distribution,* vol. 12, no. 10, pp. 2415-2424, 2018.

[42]   C. Chatri, M. Labbadi, and M. Ouassaid, "Improved high-order integral fast terminal sliding mode-based disturbance-observer for the tracking problem of PMSG in WECS," *International Journal of Electrical Power & Energy Systems,* vol. 144, p. 108514, 2023.

[43]   B. Yang, Y. Hu, H. Huang, H. Shu, T. Yu, and L. Jiang, "Perturbation estimation based robust state feedback control for grid connected DFIG wind energy conversion system," *international journal of hydrogen energy,* vol. 42, no. 33, pp. 20994-21005, 2017.

[44]   J. Wang and D. Bo, "Adaptive fixed-time sensorless maximum power point tracking control scheme for DFIG wind energy conversion system," *International Journal of Electrical Power & Energy Systems,* vol. 135, p. 107424, 2022.

[45]   P. Alinaghi Hosseinabadi, A. Ordys, A. Soltani Sharif Abadi, S. Mekhilef, and H. R. Pota, "State and disturbance observers‐based chattering‐free fixed‐time sliding mode control for a class of high‐order nonlinear systems," *Advanced Control for Applications: Engineering and Industrial Systems,* vol. 3, no. 3, p. e81, 2021.

[46]   S. Wu, X. Sun, Z. Sun, and X. Wu, "Sliding-mode control for staring-mode spacecraft using a disturbance observer," *Proceedings of the Institution of Mechanical Engineers, Part G: Journal of Aerospace Engineering,* vol. 224, no. 2, pp. 215-224, 2010.

[47]   S. Mobayen, A. Fekih, O. Boubaker, and Q. M. Zhu, "Finite-time disturbance observer-based tracking control design for nonholonomic systems," in *New Trends in Observer-based Control*: Elsevier, 2019, pp. 139-153.

[48]   S.-L. Shi, J.-X. Li, and Y.-M. Fang, "Extended-state-observer-based chattering free sliding mode control for nonlinear systems with mismatched disturbance," *IEEE Access,* vol. 6, pp. 22952-22957, 2018.

[49]   F. Nollet, T. Floquet, and W. Perruquetti, "Observer-based second order sliding mode control laws for stepper motors," *Control engineering practice,* vol. 16, no. 4, pp. 429-443, 2008.

[50]   W. Cao, Y. Xie, and Z. Tan, "Wind turbine generator technologies," *Advances in Wind Power,* vol. 1, no. 1, pp. 177-204, 2012.

[51]   M. Ragheb and A. M. Ragheb, "Wind turbines theory-the betz equation and optimal rotor tip speed ratio," *Fundamental and advanced topics in wind power,* vol. 1, no. 1, pp. 19-38, 2011.

[52]   F. Mei and B. Pal, "Modal analysis of grid-connected doubly fed induction generators," *IEEE transactions on energy conversion,* vol. 22, no. 3, pp. 728-736, 2007.

[53]   J. Liu, H. Meng, Y. Hu, Z. Lin, and W. Wang, "A novel MPPT method for enhancing energy conversion efficiency taking power smoothing into account," *Energy Conversion and Management,* vol. 101, pp. 738-748, 2015.

[54]   A. Rezaeiha, I. Kalkman, and B. Blocken, "Effect of pitch angle on power performance and aerodynamics of a vertical axis wind turbine," *Applied energy,* vol. 197, pp. 132-150, 2017.

[55]   W. Qiao, "Dynamic modeling and control of doubly fed induction generators driven by wind turbines," in *2009 IEEE/PES Power Systems Conference and Exposition*, 2009, pp. 1-8: IEEE.

[56]   R. Sitharthan, M. Karthikeyan, D. S. Sundar, and S. Rajasekaran, "Adaptive hybrid intelligent MPPT controller to approximate effectual wind speed and optimal rotor speed of variable speed wind turbine," *ISA transactions,* vol. 96, pp. 479-489, 2020.

[57]   P. Alinaghi Hosseinabadi, A. Soltani Sharif Abadi, S. Mekhilef, and H. R. Pota, "Chattering-free trajectory tracking robust predefined-time sliding mode control for a remotely operated vehicle," *Journal of Control, Automation and Electrical Systems,* vol. 31, no. 5, pp. 1177-1195, 2020.

[58]   J. Wu and X. Li, "Finite-time and fixed-time synchronization of Kuramoto-oscillator network with multiplex control," *IEEE Transactions on Control of Network Systems,* vol. 6, no. 2, pp. 863-873, 2018.

[59]   B. Osgood, "Lecture notes for EE 261: the Fourier transform and its applications," *Electrical Engineering Department, Stanford University,* 2013.

[60]   S. Yu, X. Yu, B. Shirinzadeh, and Z. Man, "Continuous finite-time control for robotic manipulators with terminal sliding mode," *Automatica,* vol. 41, no. 11, pp. 1957-1964, 2005.

[61]   Z. Zuo and L. Tie, "Distributed robust finite-time nonlinear consensus protocols for multi-agent systems," *International Journal of Systems Science,* vol. 47, no. 6, pp. 1366-1375, 2016.

[62]   X. Sun and W. Chen, "Global generalised exponential/finite-time control for course-keeping of ships," *International Journal of Control,* vol. 89, no. 6, pp. 1169-1179, 2016.

[63]   S. Parsegov, A. Polyakov, and P. Shcherbakov, "Fixed-time consensus algorithm for multi-agent systems with integrator dynamics," *IFAC Proceedings Volumes,* vol. 46, no. 27, pp. 110-115, 2013.

[64]   Z. Zuo, "Non-singular fixed-time terminal sliding mode control of non-linear systems," *IET control theory & applications,* vol. 9, no. 4, pp. 545-552, 2014.

[65]   J. M. Daly and D. W. Wang, "Output feedback sliding mode control in the presence of unknown disturbances," *Systems & Control Letters,* vol. 58, no. 3, pp. 188-193, 2009.

[66]   H. Liu, T. Zhang, and X. Tian, "Continuous output‐feedback finite‐time control for a class of second‐order nonlinear systems with disturbances," *International Journal of Robust and Nonlinear Control,* vol. 26, no. 2, pp. 218-234, 2016.

[67]   D. Zhao, S. Li, and Q. Zhu, "Output feedback terminal sliding mode control for a class of second order nonlinear systems," *Asian Journal of Control,* vol. 15, no. 1, pp. 237-247, 2013.

[68]   S. Yi and J. Zhai, "Adaptive second-order fast nonsingular terminal sliding mode control for robotic manipulators," *ISA transactions,* vol. 90, pp. 41-51, 2019.